AD-A105 604 FOREIGN TECHNOLOGY DIV WRIGHT-PATTERSON AFB OH F/G 5/2
JOURNAL OF ENGINEERING THERMOPHYSICS (SELECTED ARTICLES),(U)
SEP 81 R YAN, Z QIAN, J XU, Z JIANG, J YANG
UNCLASSIFIED FTD-ID(RS)T-0570-81 NL

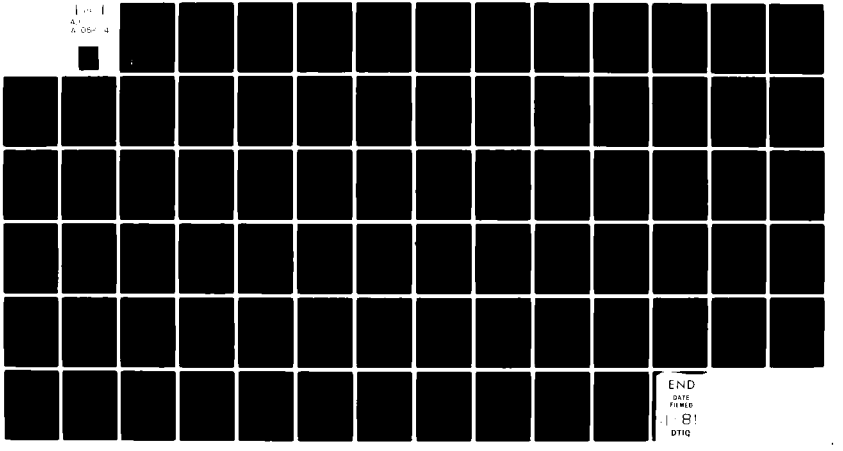

END
DATE FILMED
8 81
DTIC

FTD-ID(RS)T-0570-81

(2)

FOREIGN TECHNOLOGY DIVISION

JOURNAL OF ENGINEERING THERMOPHYSICS
(Selected Articles)

Approved for public release;
distribution unlimited.

EDITED TRANSLATION

12/79

14 FTD-ID(RS)T-0570-81

11 16 Sep [redacted] 81

MICROFICHE NR: FTD-81-C-000846

6 JOURNAL OF ENGINEERING THERMOPHYSICS
(Selected Articles)

English pages: 76

21 Source: Gongcheng Rewuli Xuebao, Vol. [redacted], Nr. 1, [redacted], pp. 6-52, 73-75, 89-91

Country of origin: (China) v2 n1 p33-42, 46-52, Feb 81

Translated by: SCITRAN
F33657-78-D-0619

Requester: FTD/TQTA

Approved for public release; distribution unlimited.

10 Ru-zun / Wang
Zhao-yun / Qian
Jian-zhong / Xu
Zu-[illegible] / Jian
Jian-sheng / Yan

PREPARED BY:

TRANSLATION DIVISION
FOREIGN TECHNOLOGY DIVISION
WP-AFB, OHIO.

1416

TABLE OF CONTENTS

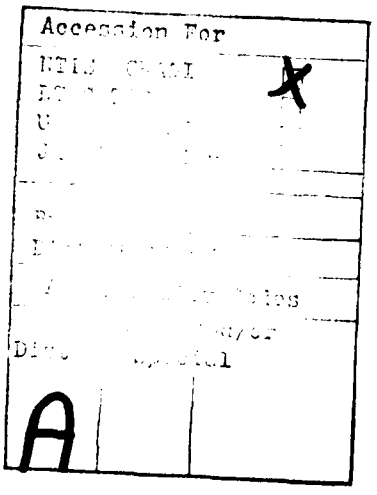

THEORETICAL INVESTIGATIONS AND EXPERIMENTAL RESEARCHES FOR HIGHER SUBSONIC TWO-DIMENSIONAL COMPRESSOR CASCADE*

Yan Ru-qun and Qian Zhao-yan
(Engine Department, North-Western Polytechnical University)

SUMMARY

The principal objective of this article is to make use of compressible turbulence flow boundary layer theory and several characteristic boundary layer parameters used in the theory of boundary layers, such as momentum thickness, form factors, energy factors and other combinational parameters of a similar sort, as well as making use of simplified gas flow speed distributions in the boundary layers in the wake behind the blade cascade and deducing, on the basis of the research foundation accumulated in the past about the theory of blade cascade losses, a simplified equation for the calculation of total two-dimensional blade cascade pressure losses for subsonic and transonic speeds. By using this equation, it is possible to make calculations of the two-dimensional blade cascade pressure losses designed operational configurations and off-designed operational configurations. In this article, the authors also introduce a new graphical method for determining the corrected gas compressibility effect in the blade cascade of compressors under operating conditions involving higher subsonic and transonic speeds.

On the basis of the formula which was deduced for the calculation of blade cascade losses, the authors carry out calculations of blade cascade losses for given blade cascade blade configurations under different operational conditions. Besides this, for given blade cascade blade configurations, the authors also carry out air flow tests in order to measure the blade cascade losses under

*This article was read at the 3rd Annual All-China Thermophysics Engineering Technology Conference in Guilin in April of 1980.

different conditions. After these two types of data are obtained, a comparision is carried out between them and this comparison reveals that the two types of data are in relatively good agreement.

THE DEDUCTION OF THE BASIC EQUATION

This article operates on the foundation of research presented in references [1,2,3] concerning the theory of the blade cascade losses in low and high subsonic speed compressors and it makes use of the theory of compressible turbulent flows and the basic principles of flow through blade cascades, that is, principles such as the conservation of energy, continuity equations, and so on, in order to deduce a formula for the calculation of the parameter of total blade cascade pressure losses $\bar{\omega}$ for comparision operating at subsonic and transonic speeds. In the process of deducing this equation, appropriate use was made of several assumptions. The total pressure losses for air flow through blade cascades is figured by making use of the average quantity of total pressure loss.

If one takes a look at Figure 1, one will see that we have determined that the measurement station at the intake of the blade cascade is cross-section 1-1. The place in the flow below the blade cascade at which the arc lengths are $1/2\sim1$ is the measurement station at the exhaust of the blade cascade which is cross-section 2-2. The average amount of total pressure loss which one finds between the cross-section at the intake of the blade cascade and the cross-section at the exhaust of the blade cascade is

$$(\overline{\Delta P^*})_1 = P_1^* - \frac{\int_{-\frac{t}{2}}^{\frac{t}{2}} \rho_2 V_{a.2} P_2^* dy}{\int_{-\frac{t}{2}}^{\frac{t}{2}} \rho_2 V_{a.2} dy} \qquad (1)$$

In this equation, P^* is the total pressure of the gas; ρ is the density of the gas; y is the tangential direction of the blade

cascade; a is the axial direction of the blade cascade; and t is the interval distance of the blade cascade.

We make the assumption that the total pressure of free flow at the intake of the blade cascade is equal to the total pressure of the exhaust of the cascade, that is to say, $P_1^* = P_{1t,2}^*$. The angle below, fs, represents the free flow, and on the basis of this representation, we can obtain

$$(\overline{\Delta P^*})_2 = \frac{\int_{-\frac{t}{2}}^{\frac{t}{2}} \rho V_{a,2}(P_{1t,2}^* - P_2^*)dy}{\int_{-\frac{t}{2}}^{\frac{t}{2}} \rho V_{a,2}dy} \qquad (2)$$

From Bernoulli's equations, $P_{1t,2}^* = p_{1t,2} + (1/2)\cdot\rho_{1t,2}V_{1t,2}^2(1+\varepsilon_1)$ and $P_2^* = p_2 + (1/2)\cdot\rho_2 V_2^2(1+\varepsilon_2)$. In these equations, $\varepsilon = (1/4)\cdot M^2 + 1/40M_1^4 + \cdots$, . M is the gas flow intake Mach number in front of the cascade.

We also make the assumption that $p_{1t,2} \approx p_2$, and on this basis, we obtain

$$P_{1t,2}^* - P_2^* = 1/2[\rho_{1t,2}V_{1t,2}^2 + \rho^2 V_2^2 + (\rho_{1t,2}V_{1t,2}^2\varepsilon_1 - \rho_2 V_2^2\varepsilon_2)] \qquad (3)$$

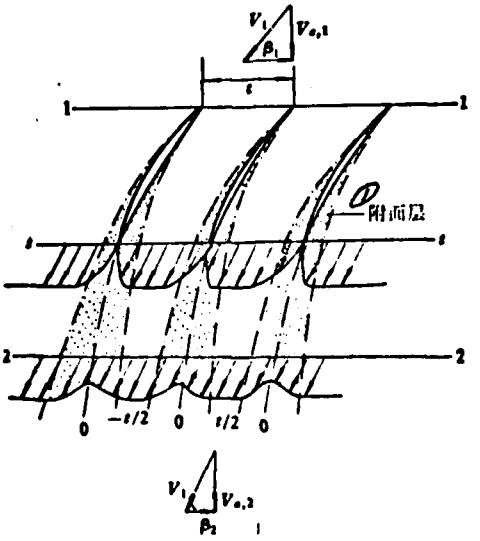

Figure 1. A schematic diagram of the boundary layer distribution along the surface of blades and of the pressure distribution in the wake area below the measurement stations in the lower part of the flow of the blade cascade.
1--boundary layer

Because of the fact that ε_1 and ε_2 in the equations above are both positive values and, in numerical terms, are both much, much smaller than 1, in order to simplify the presentation we will take Equation (3) and drop from consideration the two quantities in the small parentheses. On the basis of calculations, the error which is caused in this way is relatively small. Proceeding in this way, we obtain

$$P^*_{п.2} - P^*_2 = 1/2(\rho_{п.2}V^2_{п.2} - \rho_2 V^2_2) \tag{4}$$

If we take Equation (4) and substitute it into Equation (2), and we then do a certain amount of inferring while, at the same time, we make use of our basic knowledge concerning the theory of boundary layers, we can then obtain

$$(\overline{\Delta P^*})_2 = \frac{1}{2}\rho_{п.2}V^2_{п.2}\frac{(\theta_y/t)_2 + (\delta^{**}_y/t)_2}{(1-\delta^*_y/t)_2} \tag{5}$$

In this equation, θ is the momentum thickness of the boundary layer. δ^* is the displacement thickness of the boundary layer. δ^{**} is the energy thickness of the boundary layer.

We can write out the continuity equations for the 1-1 cross-section of the intake of the blade cascade and the 2-2 cross-section of the flow below the exhaust of the blade cascade, that is to say,

$$t\rho_1 V_1 \sin\beta_1 = \int_{-\frac{t}{2}}^{\frac{t}{2}} \rho_2 V_2 \sin\beta_2 dy \tag{6}$$

In this equation β is thw flow angle. If we take both sides of the equation above and eliminate $\rho_2 V_{п.2}\sin\beta_2$, and then go through some simple deduction, we can arrive at

$$V_{п.2} = \frac{\rho_1 V_1}{\rho_2}\cdot\frac{\sin\beta_1}{\sin\beta_2}\left(1-\frac{\delta^*_y}{t}\right)^{-1}_2 \tag{7}$$

If we take Equation (7) and substitute it into Equation (5), taking into consideration the fact that $\rho_{п.2} \approx \rho_2$, and we go through a certain amount of deduction, then we can obtain

$$(\overline{\Delta P^*})_2 = \frac{1}{2}\rho_1 V_1^2 \left(\frac{\rho_1}{\rho_2}\right)\left(\frac{\sin\beta_1}{\sin\beta_2}\right)^2 \frac{(\theta_x/t)_2 + (\delta_x^{**}/t)_2}{[1-(\delta_x^*/t)_2]^3} \qquad (8)$$

The qualitative average total pressure loss $(\overline{\Delta P^*})_2$ of the blade cascade, as it is represented by Equation (8) above very obviously shows the fact that it is a function of the characteristic parameters of the boundary layer wakes in the flow below the measurement stations on the trailing edge of the blade cascade exhaust.

In order to take the various types of characteristic wake parameters which are included in Equation (8), and by definition, put them into a perpendicular axial plane so that they are perpendicular to the direction of the flow, it is possible for one, in this case, to take these various characteristic parameters in Equation (8) and multiply them by the sine of the included angle between the planes in the direction of the free flow and the axial direction, and so obtain the desired result. At the same time, one inserts in Equation (8) a factor reflecting the configuration of the boundary layer $H = \delta^*/\theta$ and an energy factor $K = \delta^{**}/\theta$. The reason for this, the gas separation phenomenon which occurs in turbulent flow boundary layers, and this effect is controlled by changes in the numerical values of H and K. The conditions for this type of separation are very close to $H \geqslant 2.0$ and $K \approx 1.54$[4]. Besides this, we can make use of the blade cascade density $\sigma = b/t$ and the arc length b in order to express the interval distance of the blade cascade, t. If we then take the relationships set out above and substitute them into Equation (8), we can obtain

$$\overline{\Delta P^*})_2 = \frac{\rho_1 V_1^2}{2}\left(\frac{\rho_1}{\rho_2}\right)\left(\frac{\sin\beta_1}{\sin\beta_2}\right)^2\left(\frac{\theta}{b}\right)_2 \cdot \frac{\sigma}{\sin\beta_2} \cdot \frac{1+K_2}{\left[1-\left(\frac{\theta}{b}\right)_2 \frac{\sigma H_2}{\sin\beta_2}\right]^3} \qquad (9)$$

Concerning the comparison of values which this article makes between the blade cascade total pressure losses $(\overline{\Delta P^*})_2$ and the blade

cascade intake dynamic pressure $\frac{1}{2}\rho_1 V_1^2$ as measured at a station below the cascade, this comparison can be used as the total blade cascade pressure loss coefficient $\bar{\omega}$ in order to represent the flow losses in the blade cascade. At the same time, the following definitions pertain. $\tilde{\theta}_2$ is the momentum thickness parameter of boundary layers, that is to say, $\tilde{\theta}_2 = (\theta/b)_2 \cdot \sigma/\sin\beta_2$.
If one takes the two concepts mentioned above and substitutes them into Equation (9), then it is possible to obtain total pressure loss coefficient of the blade cascade involved, which is

$$\bar{\omega} = \frac{\rho_1}{\rho_2}\left(\frac{\sin\beta_1}{\sin\beta_2}\right)^2 \tilde{\theta}_2 \cdot \frac{1 + K_2}{[1 - \tilde{\theta}_2 H_2]^3} \qquad (10)$$

In order to calculate the value of $\bar{\omega}$ in Equation (10), it is necessary to establish governing principles for a flow model of the flow speed distribution in the wake of the measuring stations below the exhaust of blade cascades. In order to accomplish this, we make use of a simplified form of gas flow speed distribution model for wakes, as shown in Figure 2. In Figure 2, the vertical coordinates represent the speed ratio V/V_{fs}, and the horizontal coordinates represent the boundary layer thickness ratio $y/(\delta_{full}/2)$. In this equation, δ is the boundary layer thickness on the surface of the blades, and δ_{full} is the total boundary layer thickness above and below the blade surfaces. As far as the simplified gas flow speed distribution is concerned, it is possible to write out the form of the relationship below, that is

$$V/V_{fs} = (y/(\delta_{full}/2))^n$$

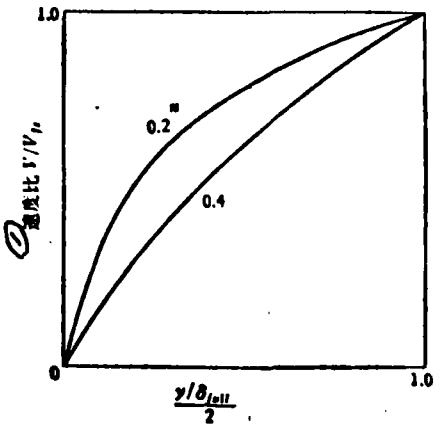

Figure 2. Simplified gas flow speed distribution model for wake.
1--speed ratio

In this equation, n is an exponent. If we are considering the case of the blade cascades of compressors in subsonic and transonic applications, then n = 0.2∿0.4. Besides this, if we are speaking of the relationship between the energy factor K and the configuration factor H as they appear in this type of simplified flow speed distribution, and if we consult references [1,2,3] in order to make use of what they present, then the relationship is $K = (H+1)/(3H-1)$. If we then take this relationship and substitute it into Equation (10), it is possible to obtain

$$\varpi = \frac{\rho_1}{\rho_2}\left(\frac{\sin\beta_1}{\sin\beta_2}\right)^2 \tilde{\theta}_2(1-\tilde{\theta}_2 H_1)^{-3}\frac{4H_1}{3H_2-1} \tag{11}$$

What one sees above is nothing more than a formula for calculating the blade cascade loss coefficient, $\bar{\omega}$, for subsonic and transonic compressors as that formula was deduced from the theory of compressible turbulent flow boundary layers. It can be seen from Equation (11) that this method of calculation can clearly be used for carrying out calculations of total pressure loss coefficients in blade cascades when those cascades are operating in a slow speed operational configuration, such as ($M_1 < 0.3$). The reason for this is the fact that, under such conditions, it is possible to recognize the gases involved as being non-compressible, that is to say, $\rho_1 = \rho_2$. In this way, Equation (11) becomes

$$\varpi = \left(\frac{\sin\beta_1}{\sin\beta_2}\right)^2 \tilde{\theta}_2(1-\tilde{\theta}_2 H_1)^{-3}\frac{4H_1}{3H_2-1} \tag{12}$$

Actually, Equation (12) is nothing else than the theoretical relationship between the total blade cascade pressure losses for low rotation speed compressors as deduced on the basis of a non-compressible flow by a consideration of Lieblein, S., and others working in a similar field as found in [2]. Besides this, it can be pointed out on the basis of references [5,6] that when one is dealing with a situation in which a blade cascade is at a high subsonic speed so that the Mach number even up to the intake in front of the

cascade reaches 1 or 1.2, then the blade trough shock loss coefficient $\bar{\omega}_s$ (no matter whether we are talking about blunt blades or sharply pointed blades) is relatively small and, in general, does not exceed an approximate value of 0.01. Because of this, generally speaking, when one gets involved with the calculation of blade cascade losses in situations in which the rotation speeds involved are high subsonic to transonic, it is possible to almost leave out shock losses inside the blade cascade from any consideration. Just as is pointed out in [7], when the intake angle of the blade cascade is increased, the blade cascade losses must also be increased; however, at such a time, the main reason for this phenomenon is not an increase in shock losses in the blade paths, but rather is primarily due to an increase in the blade form losses $\bar{\omega}_p$. The reason for this is the fact that the magnitude of shock wave losses in blade cascade paths, for all ranges of change in intake angle, do not exhibit obvious changes. Of course, it is also possible, on the basis of the method discussed in [8] to make a simple calculation of the coefficient of shock wave losses $\bar{\omega}_s$ under transonic operational conditions in the blade cascade.

Overall, what was said above is this: Concerning Equation (11) which was deduced in this article, it is possible to use it in the calculation of the total pressure loss coefficients of compressor blade cascades (whether one is dealing with blunt blades or sharply pointed blades) under designed and non-designed operational conditions of low speeds, high subsonic speeds and transonic speeds. The reason for this is that, under different operational conditions, the magnitude of blade cascade losses is generally a reflection of changes in the numerical values of various types of boundary layer characteristic parameters in the wake of the cascade involved.

Below we will discuss the quantity ρ_1/ρ_2 as found in Equation (11). This quantity is principally concerned with a consideration of the effects of gas compressibility on blade cascades under high subsonic and transonic intake speed conditions. If we give

consideration to the relationship between gas form equations and the gas kinetics total temperature and static temperature as well as total pressure and static pressure and, at the same time, assume that $P^* \approx P^*_{\text{полн}}$ and, if we also make use of the relationship $T_2^* = T_2^*$, then on the basis of all this, we can obtain

$$\frac{\rho_1}{\rho_2} = \frac{\left(1+\frac{k-1}{2}M_1^2\right)^{\frac{k}{k-1}}}{\left(1+\frac{k-1}{2}M_1^2\right)^{\frac{k}{k-1}}} \cdot \frac{1+\frac{k-1}{2}M_1^2}{1+\frac{k-1}{2}M_1^2}$$

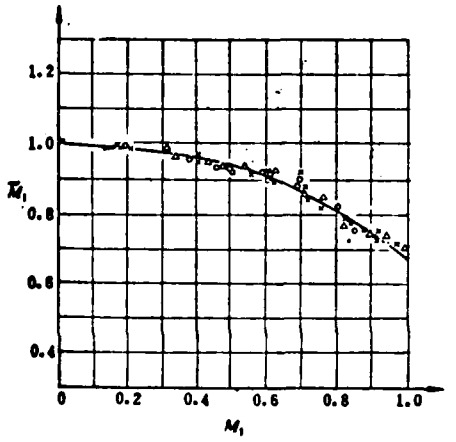

Figure 3. The curve defined by the relationship between the blade cascade intake Mach number coefficient $M_{\text{в}}$ and the Mach number M_1 of the flow coming into the blade cascade.
1--sharply pointed blade tip forms;
2--blunt blade tip forms
3--Northwestern Polytechnical University blade cascade data--Pointed blade form

△ARC RM 2794 尖头叶型; ×ARC RM 2794 钝头叶型 ○西北工业大学叶栅数据 尖头叶型

If we take the various quantities on the right side of the equation above and make a series expansion of them while, at the same time, eliminating the M number quantity for the high harmonic, then we obtain

$$\rho_1/\rho_2 = (1 - 1/2 \cdot M_1^2)(1 + 1/2 \cdot M_1^2) = \tilde{M}_1 \qquad (13)$$

The quantity $\tilde{M}_1$ in Equation (13) above is called the intake Mach number coefficient. The numberical value for the magnitude of this quantity is primarily determined by the Mach number M_1 for the flow coming into the cascade concerned. Because of this, when one is considering the time period in which the high speed gas flow is going through the blade cascade in Equation (11), he should

be concerned mostly with the influence of the compressibility of the gases involved. In this way, under operating conditions involving subsonic and transonic speeds, the blade cascade total pressure loss coefficient $\bar{\omega}$, can be written as

$$\bar{\omega} = \tilde{M}_1(\sin\beta_1/\sin\beta_l)^2\bar{\theta}_l(1-\bar{\theta}_l H_l)^{-3}\cdot 4H_l/(3H_l-1) \qquad (14)$$

Concerning the blade cascade intake Mach number coefficient $\tilde{M}_1$ as it appears in Equation (14) above, it is possible to determine its value by experimentation. Because of this fact, we took set 7 of the two dimensional experimental data for the blade cascades involved, including within it the third set of data from [9] (including data on both the blunt blade form and the pointed blade form) as well as the set four experimental data produced by Northwestern Polytechnical University for the blade cascades involved (pointed blade form) [10], and we used them in Equation (13) in order to carry out calculations. In this way, it is possible to obtain values for M_1 for different blade cascade intake Mach numbers M_1. By doing things this way, we use $\tilde{M}_1$ values as vertical coordinates and take intake Mach numbers M_1 as horizontal coordinates in order to draw out the curve defined by the relationship $\tilde{M}_1 - M_1$, as it is shown in Figure 3. From Figure 3, it can be seen that values of $\tilde{M}_1$ for different values of M_1 all fall within a relatively narrow band of data. Because of the experimental data which was employed to make Figure 3, obtained as it was from flow parameters for different blade cascade blade form geometry parameters and operational conditions, the curve $\tilde{M}_1 - M_1$ which is presented in Figure 3 is of a type which can be used relatively widely. Concerning the graph of $\tilde{M}_1 - M_1$ which we have spoken of above, it was made using a new type of method presented by the author and which corrects for the effects of compressibility of gases and various types of operating conditions involving compressor blade cascade intake speeds in the high subsonic and transonic speed ranges.

A COMPARISON WITH EXPERIMENTAL DATA

To start with, we made use of Equation (14) which expresses a formula for the total blade cascade pressure loss coefficient $\bar{\omega}$ and, on the basis of this formula, we carried out calculations for compressor blade cascades using standard blade forms under different types of operational conditions. The exponent for the simplified flow form model of gas speed sitribution in the wake of the blade cascade is n = 0.35.

Besides this, we also carried out wind flow experiments on blade cascades of the type using the standard pointed blade form and blade cascades using the blunt blade form, under both designed and off-design operational configurations. The wind tunnel experiments on blade cascades were carried out at Northwestern Polytechnical University using its two dimensional blade cascade wind tunnel. Concerning the geometrical parameters and construction of this wind tunnel, these have already been discussed in detail in [10,11]. The blunt blade $\overset{\text{model}}{\wedge}$ series which we used was the Soviet $\overset{\text{model}}{\wedge}$ 5A40/27P45 blade form. During these experiments, the range of blade cascade intake Mach numbers used was M_1 = 0.40∿0.95, and the blade cascade intake blade arc Reynolds number was $R_e \geq 4.9 \times 10^5$. Concerning the experimentation technology of this wind tunnel in terms of its automatic measurement and automatic recording systems, one can get a detailed view of all of them by consulting [12].

In Figure 4, one sees presented, for blunt blade form blade cascades under design operating conditions, the values of the total pressure loss coefficient ($\bar{\omega}_{\text{calculated}}$), which are obtained by carrying out calculations using Equation (14) and the values for the total loss coefficients which were obtained by carrying out experimental measurements as well as a comparison of the two which shows that both sets of values are in very good agreement. In Table 2, we see presented the same two types of data, that is ($\bar{\omega}_{\text{calculated}}$) and ($\bar{\omega}_{\text{measured}}$) for pointed blade blade cascades under off-design

TABLE 1. A comparison of the values of $\bar{\omega}_{calculated}$ and $\bar{\omega}_{measured}$ (design configuration of pointed blade from blade cascade)

$i = +5°$ $\frac{b}{t} = 2.05$	来流马赫数 M_1	0.4241	0.6093	0.7192	0.8207	0.8891
	2 $\bar{\omega}_{计算}$	0.0780	0.1002	0.1130	0.1532	0.2180
	3 $\bar{\omega}_{测量}$	0.0770	0.1014	0.1084	0.1529	0.2110

Key: 1--Mach number of incoming flow; 2--calculated; 3--measured

TABLE 2. A comparison of the values of $\bar{\omega}_{calculated}$ and $\bar{\omega}_{measured}$ (off-design configuration of pointed blade form blade cascade)

$i = 0°$ $\frac{b}{t} = 2.05$	1 来流马赫数 M_1	0.3920		0.6083	0.7170	0.7720	
	2 $\bar{\omega}_{计算}$	0.0519		0.0780	0.0881	0.1915	
	3 $\bar{\omega}_{测量}$	0.0512		0.0772	0.0834	0.2380	
$i = +7.5°$ $\frac{b}{t} = 2.05$	1 来流马赫数 M_1	0.3996		0.6083	0.7170	0.7720	0.8709
	2 $\bar{\omega}_{计算}$	0.0766		0.1070	0.1210	0.2150	0.220
	3 $\bar{\omega}_{测量}$	0.0810		0.1340	0.1266	0.2140	0.2360
$i = +10°$ $\frac{b}{t} = 2.05$	1 来流马赫数 M_1	0.4140	0.5074	0.6104	0.7075	0.8185	
	2 $\bar{\omega}_{计算}$	0.1153	0.1425	0.1610	0.1960	0.2050	
	3 $\bar{\omega}_{测量}$	0.1240	0.1410	0.1907	0.2750	0.2596	
$i = -2°$ $\frac{b}{t} = 2.05$	1 来流马赫数 M_1	0.3930		0.5981	0.7054	0.8000	
	2 $\bar{\omega}_{计算}$	0.0378		0.0229	0.0515	0.0563	
	3 $\bar{\omega}_{测量}$	0.0457		0.0595	0.1885	0.2280	
$i = +5°$ $\frac{b}{t} = 1.5$	1 来流马赫数 M_1	0.4140		0.6033	0.7096	0.8163	0.9189
	2 $\bar{\omega}_{计算}$	0.0515		0.0592	0.0740	0.0885	0.1210
	3 $\bar{\omega}_{测量}$	0.0483		0.0596	0.0773	0.0892	0.1680

Key: 1--Mach number of incoming flow; 2--calculated; 3--measured

operational configurations and again, the two are in relatively close agreement. In Table 3, we see presented a comparison of the same two types of data, ($\bar{\omega}_{calculated}$) and ($\bar{\omega}_{measured}$) for blunt blade form blade cascades under design operational configurations.

From the various types of data presented in Tables 1 to 3, it is possible to see that, when one is considering the type of situation in which a blade cascade is operating within design parameter ranges, the calculations which are made on the basis of Equation (14)

and the blade cascade total pressure loss coefficients $\bar{\omega}$ which are obtained by experimental measurements are both in relatively good agreement. In the case in which the blade cascade under consideration is operating in an off-design configuration (Table 2), the two types of data, $\bar{\omega}_{calculated}$ and $\bar{\omega}_{measured}$, are also relatively close. If the operational configuration of the blade cascade being considered is operating too far off the design specifications (for example, the angle of incidence is i = +10°), then the results from using Equation (14) to do calculations of $\bar{\omega}$ lose their uniformity with the measured values for the same quantity and there is an obvious discrepancy between the two. The reason for this is that, at such a time, the air flow in the passages of the blade cascade produce severe separation and in the entire blade trough one sees almost complete separation of gases. At the same time, the boundary characteristic parameters which are obtained by calculations, such as the form factor H_2 value, already approach the numerical magnitude of 2.

TABLE 3. A comparison of the values of $\bar{\omega}_{calculated}$ and $\bar{\omega}_{measured}$ (blunt blade form blade cascade in a given operation configuration).

(The row of data marked with an asterisk is a collection of the wind tunnel test characteristics for the Soviet A-40 blade).

$i = 0°$	1 来流马赫数 M_1	0.3549	0.5971	0.7149	0.8075
	2 $\bar{\omega}_{计算}$	0.0194	0.0238	0.0306	0.1135
	3 $\bar{\omega}_{测量}$	0.0241	0.0267	0.0297	0.1110
$\frac{b}{t} = 1.3$	4 $*\bar{\omega}_{特性值}$	0.0200	0.0200	0.0220	0.0390

Key: 1--Mach number for the incoming flow; 2--calculated; 3--measured; 4--collected characteristics

On the basis of what has been discussed above, if one only needs to know the total boundary layer thickness δ_{full} at the measurement station down the flow from the exhaust of the blade cascade, then it is possible, on the basis of Equation (14) to calculate the total blade cascade pressure loss coefficient $\bar{\omega}$ of blade cascades under any certain operational configuration.

It is worth while to point out that if we are carrying out new design calculations for compressor blade cascades (this does not consider the question of whether the blades involved are of the blunt type or the pointed type), then it is also possible to make use of Equation (14) in order to calculate the total blade cascade pressure loss coefficient $\bar{\omega}$ of a blade cascade in any certain operational configuration and this can be used as a reference value for use during redesigning. At such a time, it is only necessary, on the basis of the statistical data or by referring to the data calculated for a certain blade cascade in a given operational configuration, to calculate the total boundary layer thickness for the upper and lower blade surfaces, that is, δ_{full} and that will take care of everything. In Figure 4 in this article, we see graphed out the comparative values of the parameters for a blade cascade employing a certain type of geometrical parameters of blade form, that is, for both the pointed blade type and the blunt blade type, while employing different values for the angle of incidence. The values compared are the total boundary layer thickness for the blades involved, that is, δ_{full}/t, and the interval distance between the blades of the cascade, t. The ratio of these two quantities is then plotted against the experimentally measured values for the intake Mach numbers, M_1. The graphic representation of this relationship is then used as a reference in the analysis of blade pressure losses during the designing of blade cascades for compressors.

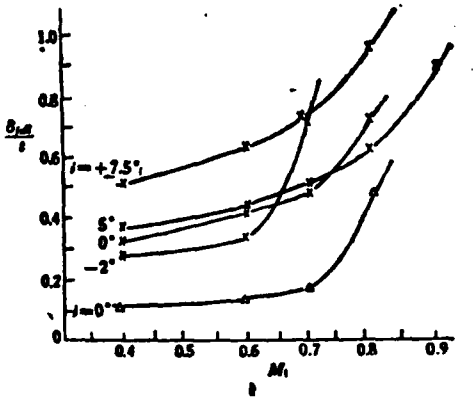

Figure 4. The curve defined by the relationship between the value of the ratio δ_{full}/t which represents the total thickness of the boundary layers involved and the interval distance between the blades for varying angles of intake incidence

Key: 1--V cross-section of an operating wheel in the second stage of a certain compressor employing pointed type blades
2--blunt type blades

CONCLUSIONS

We will now present the main conclusions which can be drawn from the material presented in this article.

1. If one makes use of the theory for boundary layers in compressible turbulence flow, employs the performance parameters which mainly characterize the boundary layers in the wake of a blade cascade and also make use of the M number for the flow coming into the cascade involved (that is, the $\tilde{M}_1$ value) as well as parameters for the geometry of the blade cascade blade being considered, then it is possible to relate these quantities to the qualitative average pressure loss coefficient for the blade cascades concerned when they are employed in subsonic and transonic modes.

2. This article makes use of the basic equation for pressure losses in blade cascades in order to deduce other theoretical relationships which are used together with a large amount of wind tunnel test data on blade cascades to present a new method of graphically representing $\tilde{M}_1 - M_1$, which is effective for blade cascades in compressors operating at high subsonic and transonic speeds and corrects for the effects of the compressibility of the gases involved.

3. The magnitude of the total pressure losses in a blade cascade is primarily dependent on the intake Mach number parameter $\tilde{M}_1$ (which is dependent on the M_1 number of the flow coming into the blade cascade) and on the value of the ratio θ_2/b between boundary layer momentum thickness and blade arc. As far as the boundary layer energy factor K_2 or the configuration factor H_2 go, they are secondary in their influence on the total pressure losses in a blade cascade.

4. If we consider a certain given blade cascade operating under a certain type of configuration, then if we already know or can estimate the total boundary layer thickness on the surface of blades down the air stream from the exhaust of the cascade being considered, then it is possible to calculate the qualitative average total pressure coefficient for the cascade being considered, that is, $\bar{\omega}$ (including both design operational configurations for the blade cascade being considered and off-design operational configurations).

REFERENCES

[1] Stewart, W. L.: Analysis of Two-Dimensional Compressible-Flow loss Characteristics Downstream of Turbomachine Blade Rows in terms of Basic Boundary-layer Characteristics, *NACA TN 3515*, (1955).

[2] Lieblein, S. and Roudebush, W. H.: Theoretical loss Relation for low Speed Two-Dimensional Cascade Flows, *NACA TN 3663*, (1956).

[3] Lieblein, S. and Roudebush, W. H.: Low-Speed Wake Characteristics of Two-Dimensional Cascade and Isolated Airfoil Sections, *NACA, TN 3771*, (1956).

[4] Schlichting, H.: Application of Boundary-Layer Theory in Turbomachinery, *Trans. ASME 81D*, (1959).

[5] Koch, C. C. and Smith Jr., L. H.: Loss Sources and Magnitude in Axial Flow Compressors, *Trans. ASME Series A*, 96, 3, July, (1976).

[6] Heilman, H., Starken, H. and Weger, H.: Cascade Wind Tunnel Tests on Blade Design for Transonic and Supersonic Compressors, *AD 637837*, Sept. (1968).

[7] Dowis, G. W. and Hartmann, M. J.: Shock Losses in Transonic Compressor Blade Rows, *Trans. ASME 83A*, (1961).

[8] Swan, W. C.: A Practical Method of Predicting Transonic Compressor Performance, *Trans. ASME Series A*, 83, 1961.

[9] Todd, K. W.: An Experimental Study of Three-Dimensional High Speed Air Conditions in a Cascade of Axial Compressor Cascade, *AEC RM 2794*, (1954).

[10] Blade Cascade Experimentation Team: "Experimental Research on Plane Blade Cascades in Order to Determine the Effects of Backward Sweep", Northwestern Polytechnical University, Scientific and Technological Materials Syllabus, No. 634, 1968.

[11] Blade Cascade Experimentation Team: "Plane Blade Cascade Wind Tunnels", Northwestern Polytechnical University Press, 1977.

[12] Qian Zhao-yen: "Automatic Recording and Data Processing in Wind Tunnel Test Technology Relating to Plane Blade Cascades", Northwestern Polytechnical University, Scientific and Technological Materials Syllabus, No. 1076, 1979.

THEORETICAL INVESTIGATIONS AND EXPERIMENTAL RESEARCHES FOR HIGHER SUBSONIC TWO-DIMENSIONAL COMPRESSOR CASCADE

Yan Ru-qun, Qian Zhao-yan

(Engine Department, North-Western Polytechnical University)

Abstract

The losses occured in air-flow of compressor cascade are mainly to be controlled by occuring developing and separting of boundary-layer on the surfaces of blade. Therefore, by means of adapting the theory of compressible turbulent boundarylayer, utilizing some characteristic parameters such as momentum thickness, form factor, energy factor and other combination parameters, and then supposing the flow model of simple power of velocity distribution in the wake behind the cascade, a simplified calculating equation for total pressure loss coefficient of subsonic and transonic cascades of the compressor is derived. The basic calculating equation derived would be used for predicting the total pressure losses of both design condition and off-design condition of the compressor cascade.

In this paper, a new curvilinear method for correcting the gaseous compressible effect under higher subsonic and transonic intake condition upstream of the cascade is presented.

According to this basic equation, the total pressure losses for given compressor cascade are calculated, and then tested on the plane wind tunnel at various conditions, both the results are in better agreement.

THE SHOCK WAVE STRUCTURE AND THE ANALYSIS OF THE FLOW THROUGH TRANSONIC TURBINE CASCADES*

Min Da-fu
(The Qing Ho Aerodynamic Lab. of the Beijing Heavy Electrical Machine Works)

SUMMARY

On the basis of Schlieren photographs which were taken during tests run on plane blade cascade air flow during transonic turbine operation, an analytical discussion is carried out on the subject of shock wave structure and development in exhaust flow fields and blade cascade paths. On the basis of the results of these experiments, we verified the existence of shock wave deflection on free boundary surfaces as well as the influence of this phenomenon on the convection flow characteristics. In the third section of this article, we carry out a discussion of several classic types of the phenomenon of interference between shock waves and boundary layers.

1. FOREWORD

The shock wave system structure in the passages of plane blade cascades as used in transonic turbine applications and in exhaust flow fields as well as the interference between these shock waves and the boundary layers involved determine, to a very large extent, the flow characteristics of a blade cascade. In order to do research on the design principles of transonic blade cascades for the purpose of developing blade cascades which do not produce shock waves, it is necessary to make very careful observations and analyses of the shock wave structures involved in winding flow fields. Our laboratory carried out experiments on several sets of blade cascades as

* This paper was read at the Third Annual All-China Engineering Thermophysics Technology Conference in Gui Zhou, April 1980.

well as taking Schlieren photographs to correspond with these cascades during the course of the experiments. The results of the experiments showed that when the exhaust M number approached 1, that shock waves appeared in the passages of the blade cascades involved as well as in the exhaust flow fields. When this M number was extended somewhat more, the strength of the shock wave involved as well as their positions exhibited changes. Reference [1] has already documented and discussed these problems and this article will take the discussion of models for the shock wave systems under consideration a bit further on the basis of the results of experimentation.

Concerning plane blade cascade wind tunnels, due to the fact that the blades are very limited, in the flow from the first blade to the last one, there exist on the boundaries of the flow free boundary surfaces. The outside tail shock waves produced by the trailing edges of the blade cascades being considered will produce, on the free boundaries, deflections and the formation of complex systems of shock waves. Varying with changes in the M number, these types of complex structures will also exhibit changes. [2] has already given its main attention to this question. It can be verified from the Schlieren photographs of the several blade cascades which went through testing in our laboratory that this sort of phenomenon does exist and we will set out from the basic principles of gas flow dynamics to arrive at a solution of this problem area. The essence of this problem is that, due to the deflection which takes place with this type of shock wave, one gets the formation of multi-peak type parameters and wave forms in the exhaust flow fields of turbine blade cascades in transonic applications. These types of multi-peaked forms also exert an influence on our evaluation of the aerodynamic performance of blade cascades. This article will take the results of aerodynamic experiments and the available Schlieren photography in order to analyze and solve this problem.

The interference between shock waves and boundary layers is an important factor affecting turbine blade cascade pressure losses in transonic applications as well as other performance characteristics. From Schlieren photographs, we can obtain some enlightenment on the subject of how to solve the problem of this physical phenomenon. However, due to the excessive complexity of the problem, it is difficult even from the photography which we already have to reach firm conclusions concerning this problem and we still must wait upon continued efforts in the future.

2. EXPERIMENTAL EQUIPMENT AND METHODS

All the experimentation which we did was carried out on the FOlintermittent type transonic turbine blade cascade wind tunnel [3]. The Schlieren photography was done by making use of a 505-I type Schlieren apparatus [4] and the camera employed was a type DF-7 Seagull brand. The speed selected for the photography was 1/500 sec^{-1}. During the time when the photography was being done, the semi-circular dish in the experimental section of the wind tunnel was modified to include organic glass observation windows. Given this modification, the installation plate for the blade cascade, due to strength and equipment capabilities, could not help but make use of organic glass in its manufacture and due to flaws in the optical capabilities of these windows, the clarity and precision of the images of the gas flow in the passageways of the blade cascade involved fall somewhat short of what could otherwise be expected.

Based on the principles governing the formation of Schlieren images, it is only when one has had a density gradient in the direction of the normal line of the cutting edge of a blade that it is possible to get the production of a clear and precise image. Because of this, if we take the knife edge and position it in a direction perpendicular to the gas flow in the exhaust, then it will be possible to take more completely satisfactory pictures of the shock wave systems under study. Moreover, when the knife edge is

placed in a direction parallel to the direction of the gas flow, then it is possible to achieve even clearer and more precise pictures of the wakes present.

3. EXPERIMENTAL RESULTS AND ANALYSIS

1. The formation and development of the shock wave systems in the blade cascade passageways

Figure 1 consists of Schlieren photographs of certain blade cascades under various operating conditions. From these photographs, it is possible to see how shock wave systems are set up under various different operational situations.

As far as turbine blade cascades are concerned, in operating conditions involving high subsonic speeds, one will get the production of localized areas of supersonic speeds inside of the passages. These sonic speeds first reach a place somewhere on the back parts of the blades and then form a boundary line on which $M = 1$ within the passages. The lower reaches of this sort of line reach from the convex surface of the backs of the blades and product a series of expansion waves which cause the speed to be increased somewhat more. This creates an area in which $M > 1$. Within this area, the extraneous reflections which are cast unto the boundary plane $M = 1$ by the expansion waves return to the solid wall of the back of the blades as compression waves. These compression waves, after they make homogeneous reflections on the solid wall surface, form type λ shock waves. Because of this fact, this localized area of supersonic speeds takes $M = 1$ as its front boundary and the other boundary of this small area--in the rear--is the λ type shock wave itself. This type of phenomenon is represented quite clearly and precisely even in Schlieren photographs in which M is approximately 0.9. Figure 2 is a model of this type of flow.

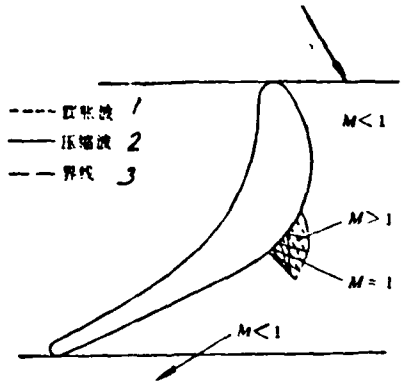

Figure 2. A flow model of localized areas of supersonic speeds under subsonic operational conditions

Key: 1--expansion wave; 2--compression wave; 3--boundary line

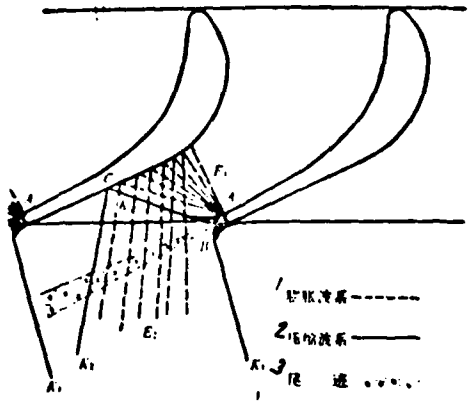

Figure 3. A diagram of the chamfer section of a wave system in a transonic planar blade cascade under supersonic operating conditions.

Key: 1--expansion wave system; 2--compression wave system; 3--wake

After the gas flow passes through such localized areas of supersonic flow, it continues to move along the passageways and in the vicinity of the exit, due to the curvature of the trailing edges of the air flow, it increases speed. In such a situation, it is easy (particularly on the backs of the blades in the exhaust) to produce localized areas of supersonic speeds.

When the pressure ratio behind the pressure in front of the blade cascade being considered and the pressure behind it drops to the critical level for that ratio, then the chamber portion of the passageways involved will be formed into a supersonic wave system. The model for the flow in this system is shown in Figure 2.

The wave system inside the passageways and the exhaust flow field is made up of the original expansion wave, E_1, the reflected expansion wave, E_2, the interior wake wave, K_1, the reflected wave of the interior wake wave, K_2, the exterior wake wave, K_3, as well

as the wakes from the trailing edges of the blades involved. After the back pressure drops below the critical pressure for that quantity, the throat section of the passageway involved will reach the speed of sound, the pressure at the end point of the interior arc, A, will be the critical value and in order to reach a certain back pressure, it is necessary to produce at that point a set of expansion waves, E_1. This type of expansion wave extends directly to the back arc of the neighboring blades and from there is reflected out as the set of expansion waves, E_2. The gas flow, from the back arc and interior arc of the blade surfaces involved, bends out around the trailing edges. Moreover, at a certain point B at a given distance from the trailing edges, these flows will come together. Due to the fact that the gas flow takes a violent turn in the vicinity of this point B, it simultaneously produces two sets of compression wave systems, composed of a swallow tail wave system, that is to say, the interior wake wave, K_1 and the exterior wake wave, K_3. The interior wake wave has an effect on the point C on the back of the blade form and mutually interacts with the boundary layers involved. After this interaction, the shock wave, K_2, is reflected back out. This shock wave is a function of the increase in the M number at the exhaust. Concerning the increase in strength of E_1 and E_2, K_1, at the point where the jet enters the back of the blade form, moves in the direction of the exhaust profile. When the E_1 expansion wave system puts its last wave in a basically parallel condition with the cross-section of the exhaust, then it is possible to recognize the fact that we have reached the extreme limit of the blade cascade involved.

The reflection which takes place from a wave system which is reflected off a solid wall is a reflection which retains the form of the original, that is to say, that the reflection of an expansion wave is an expansion wave. After the reflection of a shock wave, the reflected wave will still also be a shock wave. This point is not only capable of being verified from the principles of

aerodynamics [5,6]; it is also completely verified by the Schlieren photographs which we took. In the flow field of the exhaust, two sets of shock waves usually intersect. If the two sets which intersect are compression waves of a similar type, then after they intersect, they come together to form one shock wave set. This type of situation is shown in its most standard form in Plate 1, where the reflected wave, K_2, which is the result of the interior wake wave, K_1, being in contact with the solid wall surface, and the exterior wake wave, K_3, come together (see Figure 4a). The situation in which shock waves of different types intersect is different. Generally speaking, the common situation is one in which the two shock waves involved just penetrate each other. If the strength of the two shock waves is equal, then, after the penetration, they form a simple crossed-fork pattern, which is a symmetrical pattern. If the strengths of the two are not equal or their M number is relatively small, then the vicinity in which these two sets of shock waves intersect will be turned into a small section of straight shock wave. The whole wave system will present the appearance of a bridge-shape. It is worthwhile to point out that, due to the fact that shock waves of different strengths are being crossed, the gains in enthalpy are not the same either. When the gas flow penetrates two sets of waves, the speeds of the top and bottom two halves will be different (although, at the same time, the pressures and directions of flow for the two parts will still be the same). Because of these facts, there will exist in the center a non-continuous vortical surface (see Figure 4b). The gas flow model for an intersection between shock waves is as shown in Figure 4. The one on the right side is the Schlieren photograph which corresponds to this. On the basis of the discussion above and the analysis presented there, it is possible to easily understand Plate 1, which is a set of Schlieren photographs which present wave systems under different operational conditions.

2. <u>The form of reflected shock waves and the influence of their convection flow characteristics</u>

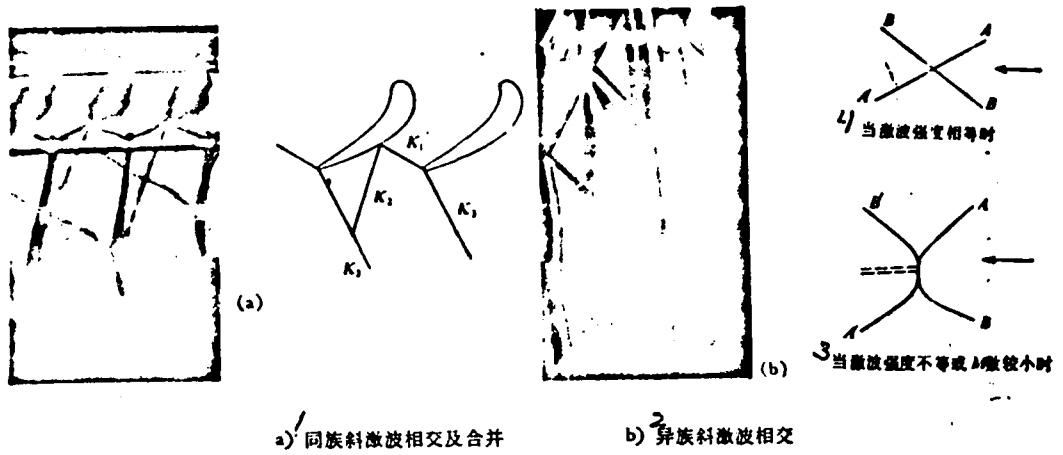

Figure 4. An aerodynamic model for the intersection of shock waves and the Schlieren phtographs for it.

Key: 1--the intersection and remerging of sloped shock waves of a similar type; 2--the intersection of sloped shock waves of different types; 3--when the strength of shock waves is not the same or the M number is relatively small; 4--when the strengths of the shock waves are equal.

Concerning blade cascade wind tunnels, due to the fact that the number of blades is very limited, the exhaust flow field must contain two free boundary lines. It can be clearly shown from the Schlieren photographs which we took that in the reflection of a shock wave from a free boundary, there is a new shock wave produced. This phenomenon was noticed early on by NACA [7] and research was done on it in 1968 by Von Karman. C. Sieverding [2] has also given his attention to this problem.

Concerning the phenomenon discussed above, the experimental diagram which we produced can be explained as follows. When the exterior wake shock wave gets close to the free boundary surface, one sees formed an area of transition from supersonic to subsonic speed. Inside of this area, the M number gets gradually smaller; moreover, this slowing is accompanied by the production of vortical surfaces and an increase in enthalpy. As a result of this, one sees the shock wave involved gradually exhibit curvature. In order to maintain the equilibrium of the flow, within the transition area

close to the exterior wake shock wave curvature, there will be produced a new shock wave. The Mach number reflection limits for this model and the classic model are both similar. The latter usually has a Mach number of flow relatively close to 1 and occurs when the angle of folding is relatively large. Of course, in order to maintain the condition of equal pressure on the free boundary surface, in the lower part of the entering shock wave, there is also a set of expansion shock waves sent out. It can be seen from the Schlieren photography in plate 1 that:

1. In the range of $M_{2n} = 1 \sim 1.1$, the wake area produced by the exterior wake shock wave, K_3, going through the blade wake area gives rise to a weak reflected shock wave. In response to a reduction in the ratio of the pressure in front of a blade cascade and the pressure behind it, the speeds in evidence at various points in the flow field behind the exhaust of the blade cascade will be increased; then the point at which the reflected shock wave is produced will gradually get closer to the free boundary surface.

2. These reflected shock waves always return to sections of blade cascade passage but some sections of these passages still do not have this type of wave. Because of this, the periodicity of the passageways is disrupted.

3. Following an increase in the M number at the exhaust, the direction of the exterior wake shock wave manifests a change. The direction of its reflected shock wave also changes in response to this and the more the process continues the more the direction of the reflected shock wave becomes parallel to the profile line of the exhaust. The passageways which feel the influence of the reflected shock waves also decrease in size in response to these other changes.

Concerning the existence of free surface reflected shock waves, these shock waves interfere with the passageways of the blade

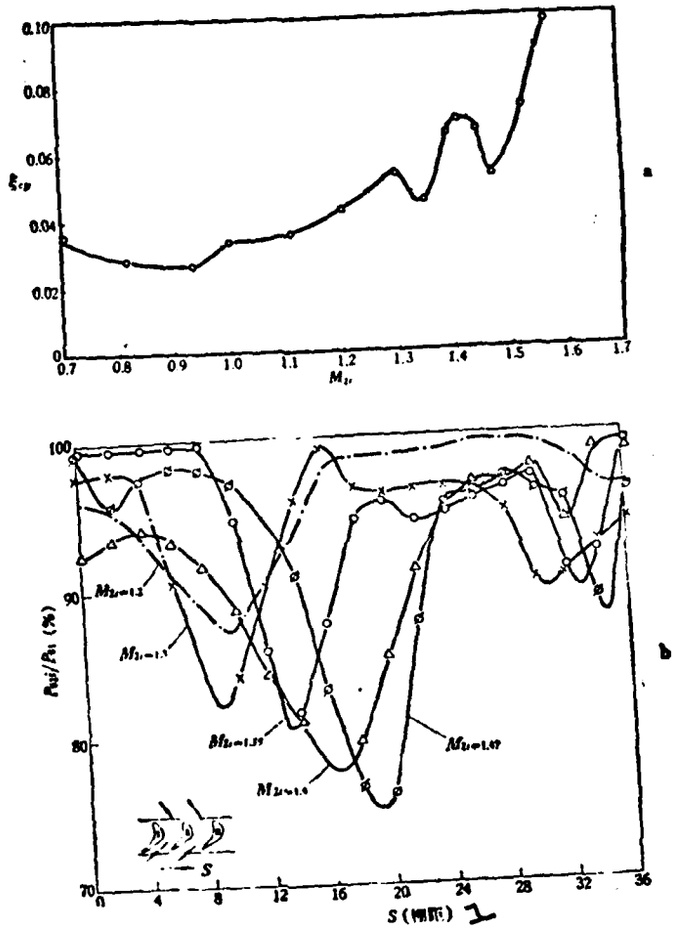

Figure 5. Experimental Curves for Transonic Turbine Blade Cascade Performance.

a) $\xi \sim M_{1t}$ curve b) $P_{01}/P_{01} \sim S$ curve

1 - cascade interval

cascades involved and with the periodicity of the exhaust flow field and this creates a false appearance in some areas which has some influence on the reliability of the blade cascade wind tunnel data from time to time. Figure 5 is a display of the aerodynamic characteristics of a certain blade cascade. In it, a) is the relationship according to which the loss coefficient ξ changes as a function of M_{2t}. In the same diagram, b) is a distribution diagram of total pressure as actually measured at various distances along the blade cascade for increments of M_{2t}. In can be seen from b) in this diagram that the cascade losses are composed of two parts. From left to right, the first loss area is that formed by the wake. The second loss increase area is the result of the influence of the wake edge shock wave. If we consult plate 1's Schlieren photographs, when $M_{2t} = 1.3$, there is a mutual influence between the reflected shock wave from the free boundary and the exterior wake shock wave of blade cascade II. This effect causes an enlargement of the second loss area. Because of this fact, there is an obvious increase in losses (see Figure 5a). When M_{2t} is is raised to 1.35, the reflected shock wave moves toward the outside of the blade cascade, leaving the passageways, and causing losses instead of drops. When M_{2t} is raised to reach 1.4, the reflected shock wave reaches the back portion of blade II which is being measured causing localized boundary layer separation. There is a clear enlargement of the wake loss area and the amount of loss is again increased. When the process of increase is continued straight on until $M_{2t} = 1.47$ or thereabouts, the reflected shock wave involved moves out of the back

portion of the blade being measured and the losses drop again. After this, following an increase in the M_{2t} number, the reflected shock wave reaches a direction which tends to be parallel to the profile line of the blade cascade being considered. The influence on the performance of the passageways tends to disappear. However, due to an increase in the strength of the shock waves, the interior wake shock wave again exerts its influence on the subsonic area at the trailing edge and there is a sharp increase in the amount of losses experienced. From the analysis advanced above, it can be seen that the loss curve for waves within the range $M_{2t} = 1.3$ to 1.47 can very possibly be a false image produced by the shock wave

reflected from the free surface. It was also discovered during these experiments that the exhaust angle of the blade cascades being considered in this section of the operational ranges also exhibits wave movement and can almost be explained by the use of this reason.

In order to raise the reliability of the data, speaking in terms of basics, one needs to find a method for eliminating this reflected shock wave phenomenon. Quite a few scholars have put a lot of effort into this problem, coming up with such solutions as making use of perforated walls with or without suction, using movable final blades and other such measures. However, the results from these attempts have not been too impressive. Looking at the problem from another angle, if one were able to create a mechanism by which to carry out in-depth studies of reflected shock waves, then from this basis it might be possible to carry out calculations of and adjustments for the influences of blade cascade aerodynamic characteristics as modified by reflected shock waves. This would also make it possible to some extent to eliminate the deficiencies of transonic planar blade cascade wind tunnels. In fact, because of the fact that the position which corresponds to the measurement point on the shock wave involved is different for each blade cascade, the influence which the shock waves will have on the construction of different blade cascades will also certainly not be limited to only one kind. In our opinion, before we will be able to clearly understand the laws which govern this type of phenomena and before we make precise experimental determinations of the characteristics of each different type of blade cascade as far as this problem is concerned, it would be very useful to the objective of raising the reliability of our data to continue on resolutely with the taking of Schlieren photographs in order to see clearly the locations and functioning of reflected shock waves and exert every energy toward the choosing of appropriate passageways and positions for the construction of blade cascades.

3. Interference between shock waves and boundary layers

From the Schlieren photograph in plate 1, it is possible to see that there are several types of interference phenomena occuring between shock waves and boundary layers. In the interval when $M_u = 1.0 \sim 1.2$ the internal wake shock wave of the III blade shoots into the back arc of the II blade and sends out two shock waves. This phenomenon is the result of interference between shock waves and boundary layers. From (8) one can know that the design of this set of blade cascades in its constriction section is relatively good and the gas flow along the back arc of the blade forms accelerates uniformly. Due to the fact that the acceleration of the flow has a stabilizing effect on the boundary layers involved, the laminar flow flow configuration is capable of maintaining itself up to a very high critical Reynolds number $(Re^{**} = 1.0 \times 10^6)$[9] Because of this fact, within the range of our experimentation, the boundary layers of the backs of blades can still be considered as laminar flows.

As is shown right in Figure 6, when the interior wake shock wave enters into the laminar flow of a boundary layer, it applies to the boundary layer a positive pressure gradient. This type of pressure gradient, in the subsonic flow layer inside of the boundary layer, flows toward the upper reaches of the flow to propagate itself. At the places where this shock wave enters the upper reaches, it causes the beginning of an increase in pressure strength. This type of pressure strength comes back around and is again capable of leading to an increase in the thickness of the boundary layer involved. Because of this leading to localized changes in the rate of curvature of the flow lines involved, a system of compression waves is produced. This system of compression waves follows behind and comes together to form the first reflected shock wave. It is possible to see that the point of origin of the first reflected shock wave should be in the upper reaches of the flow where the original point of entry was. Due to the fact that gas flow outside

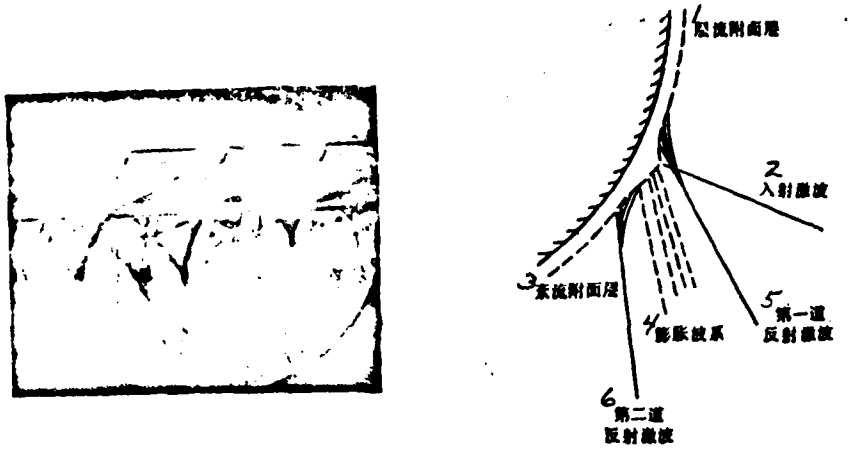

Figure 6. A model of the interference which takes place between shock waves and boundary layers as well as a Schlieren photograph of its typical form.

Key: 1--laminar flow boundary layer; 2--the incoming shock wave; 3--turbulence flow boundary layer; 4--expansion wave system; 5--the first reflected shock wave; 6--the second reflected shock wave

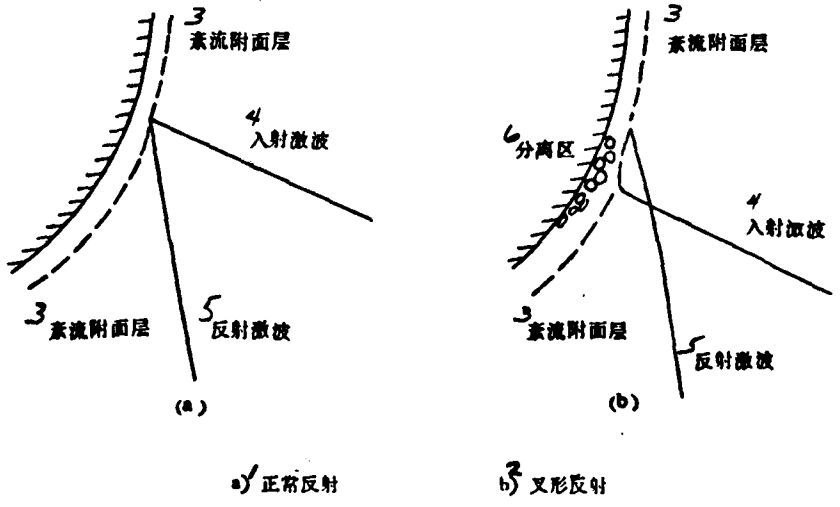

Figure 7. A flow model of the interference between shock waves and boundary layers.

Key: 1--normal reflection; 2--fork-type reflection; 3--turbulence flow boundary layer; 4--shock wave entry; 5--reflected shock wave; 6--area of separation

of the boundary layer penetrates the shock wave at points where its pressure strength is larger than that in the boundary layer, the pressure strength gradient which this creates will again cause a folding back of the flow lines toward the wall surface and will lead to an increase in the curvature of the surface of the blade being considered. From all of this comes the production of a set of expansion waves that constitute a system. However, very frequently, due to the fact that the angle of deflection of the expansion waves is too great, this tends to cause the air flow to move in toward the wall surface and the wall surface further down has an effect of adjusting the direction of the gas flow. It is as if one had a concave angle there leading to the production of a system of compression waves which later come together to form the second reflected shock wave. Following hard on after the second shock wave, the boundary layer follows along and turns to become the turbulence flow. Figure 6 is a model of the interference between shock waves and boundary layers as well as a Schlieren photograph of the typical form of this phenomenon.

When a shock wave makes its effects felt in a turbulence flow boundary layer, the situation is very much different. Due to the fact that the turbulence flow boundary layer is capable of relatively well overcoming the reverse pressure gradient, the effects produced by the interference are much smaller. At this time the thickness of the boundary layer involved increases only very slightly. In the flow above and below the point of entry, one will see the production of several beams with very small ranges of influence. Because of all this, the reflection of shock waves in a turbulence flow boundary layer closely approximates a normal reflection, that is to say, the angle of entry of the shock wave and the angle of reflection will be approximately equal. The model for this type of flow is as shown in Figure 7a. The corresponding Schlieren photographs are as shown in plate 1 for the $M_{2t} = 1.3 \sim 1.35$ situation.

When M_{2t} continuously increases, the strength of the entering shock wave increases. The effect which the entering shock wave will have on a turbulence flow will cause the occurrence of a small amount of separation. The reflected shock wave which occurs at this time will begin from the point of entry and spread up the flow forming a fork-type reflected shock wave as shown in Figure 7b. The Schlieren photograph for this type of reflection can be seen in plate 1 as the situation in which $M_{2t} = 1.4$.

Due to the fact that the interference between shock waves and boundary layers is a type of irregular, complicated physical phenomenon, at present, in the pictures which are taken of turbine blade cascades in transonic applications still lack clarity. When we went through the Schlieren photographs for this set of blade cascades, it was only possible to make a few very crude observations and come to some crude understandings of these phenomena.

The analysis and editing involved in this article were done by Min Da-fu.

REFERENCES

[1] Qing Ho Laboratory of the Beijing Heavy Electrical Machine Works: Experimental Research on the Aerodynamics of the Planar Blade Cascades of Transonic Turbines-Wind Tunnel Experiments on the Center Cross Sections of Blades 850mm long (Operational Report), 1978, March.

[2] C. Sieverding: Transonic Turbine Blading, AGARD CP-34 Part II, (AD 887774).

[3] Qing Ho Laboratory of the Beijing Heavy Electrical Machine Works: An Explanation of the Design of the F-01 Transonic Blade Cascade Wind Tunnel, Jan 1975.

[4] Jin Zhou Optical Equipment Works: Instructions for the use of the Model 505-I Schlieren Device.

[5] H. Shapiro: The Aerodynamics of Compressible Flows and Thermophysics (Vol. I and II), Science Publishing House, 1966.

[6] M. Ye. Deych: Engineering Aerodynamics, Fuel Industry Publishing House, 1955

[7] Cavour, H. Hauser: Study of Flow Conditions and Deflection Angle at Exit of Two-Dimensional Cascade of Turbine Rotor Blades at Critical and Supercritical Pressure Ratio, NACA RM E9K25.

[8] Qing Ho Laboratory of the Beijing Heavy Electrical Machine Works: Transonic Wind Tunnel Research on Blade Cross Sections of the 518mm Blades of the 100,000 Watt One Cylinder Gas Turbine (Operational Report), 1978.

[9] Е. В. Майорский: Экспериментальное сверхвукового потока в турбинных решетках, Теплоэнергетика, 1965, №. 12

THE SHOCK WAVE STRUCTURE AND THE ANALYSIS OF THE FLOW THROUGH TRANSONIC TURBINE CASCADE

Min Da-fu

(The Aerodynamic Lab. of the Beijing Heavy Electrical Machine Works)

Abstract

Throughout a lct of Schlieren photos from the aerodynamic experiments of the Transonic Tunbine cascade, the mechanism of the generation and development of the shock waves in channel and exit flow field of the cascade is studied. In these photos, there are a series of deflect shock waves from the free boundary of the jet, Passing through the analysis of this physical phenomenon, the satisfied explanation on the aerodynamic performance which has a multipeak type of curve is obtained. In the 3rd of this article, three types of interaction between shock waves and boundary layer are observed and discussed simply.

A THEORETICAL ANALYSIS OF THE STREAM SURFACE OF REVOLUTION WITH SUPERSONIC INLET FLOW IN A TRANSONIC AXIAL COMPRESSOR*

Xu Jian-zhong, Jiang Zuo-ren, Yang Jin-sheng, Zhang Ying and Du Zhuan-she
(Institute of Engineering Thermophysics, Academia Sinica)

If we start with changes in the direction and numerical value of the speeds corresponding to gas flows when going through a shock wave as these changes lead to jumps in the absolute speeds of gas flows as well as to jumps in the tangential components of these gas flows, one should make use of planar oblique wave relationships to establish a formula for expressing $\Delta(V_{\theta r})$, losses and total pressure ratios and from the applicable theory, we explained the important phenomena related to gas pressure increases when passing through shock waves. We considered the results of experimentation, assumed the positions at which shock waves were crossed as well as their configurations and made use of the characteristic curve method in the intake area. We also made a theoretical analysis of the surface of revolution of the supersonic intake. From this analysis it could be seen that there were several special points associated with transonic compression and compressors. Calculations also showed that in the center line exhaust, when the inverse problems of the velocity moment $V_{\theta r}$ and the S_2 flow are calculated, the numerical values which are arrived at for the two are very close. If one arranges, for the blades involved, the average results of calculating regular values of S_2 and the Mach number distributions which are obtained by substituting into the S_2 flow surface calculations the flow filament thickness and the $V_{\theta r}$, $\Delta i/R$ which are gotten by considering the shock waves involved, then there will be a particularly large difference between conditions in front of the shock waves involved and the conditions behind them.

*This article was read at the 3rd Annual All-China Engineering Thermophysics and Technology Conference held in Gui Lin in April of 1980.

1. FOREWORD

In order to make an in-depth study of the complex three-dimensional flows inside of transonic axial-type compressors, we took its aerodynamic and thermodynamic design as offering a reliable theoretical foundation and on the basis of the theory and methods presented in [1], we designed a single-stage research compressor [2].

As far as transonic flows which carry shock waves with them are concerned, there are two methods of understanding them. One type of method is to do numerical calculations and obtain the whole flow field after one has established a physical model and set up the necessary mathematical equations as well as establishing the conditions for the solutions desired. When this type of solution is employed, the jumps in the parameters behind the wave are replaced by continuous changes and the shock wave is pulled apart into two or three coordinate networks. The other method is to assume the position and configuration of the shock waves involved and solve for the flow fields in front and behind them. The calculations involved in this type of solution are relatively simple. The key to using this method is the accuracy of the determinations for the position and configurations of the shock waves involved and these quantities need to be determined by experimentation.

References [3,4] make use of the laser method for measuring speed. These references carry out relatively detailed measurements of the flow fields of transonic axial compressors which contain shock waves in them and make a comparison between these results and the results obtained by normal measurement and flow calculation techniques. These references obtained quite a few interesting results.

In order to analyze the effect which shock wave have on gas flow, this article starts with changes in the gas flow velocity

triangle behind the shock wave being considered, then use is made of the planar oblique relationship formula and we deduce the corresponding values of $\Delta(V_{on})$, pressure losses and total pressure ratios which are expressed by this type of formula. This explains the important phenomenon involved when the supersonic intake cross-section shock waves of transonic compressors cause additional pressurization of gas flow or "supercharging". On this foundation, we consult the results of experimentation, assume certain positions and configurations for the shock waves involved. We then carry out aerodynamic and thermodynamic analyses and calculations on the top cross-sections of the rotors in [2] and then discuss the results obtained.

2. CHARACTERISTIC CURVE CALCULATIONS FOR THE SHOCK WAVES IN FRONT OF BLADE CASCADES AND FOR THE INTAKE AREAS OF THESE CASCADES

In order to carry out aerodynamic and thermodynamic calculations of the intake surface of revolution and supersonic conditions, it is necessary to accurately know the position and configuration of the shock wave in front of the blade cascade involved. In this regard, as far as isolated wing forms are concerned, we already have, on the basis of experimental data, the relatively easily adaptable MOECKEL model [5]. Obviously, as far as blade cascades in compressors are concerned, one should give consideration to the lack of uniformity in the flow fields of the upper reaches of the flows involved. Other such factors should also be similarly considered in the light of their influence on the make-up of the position and configuration of shock waves in front of blade cascades. These other factors are such things as the mutual interaction between blades and the structure of the blade cascade itself.

Concerning a rotational supersonic intake area from behind a detached shock wave to the passageways in front of the shock waves, it is possible to make use of the characteristic curve method in order to solve for the quantities desired. Reference [6] gives us

a characteristic curve equation which includes the flow filament thickness τ and the redius r of the surface of revolution as well as other relationships on which this equation is based, that is

$$\lambda_{1,2} = \left(r\frac{d\varphi}{dl}\right)_{1,2} = \frac{K}{J} \mp \frac{\sqrt{K^2 - JL}}{J} = \operatorname{tg}(\beta \pm \alpha)$$

$$\frac{1}{W}\left(\frac{dW}{dl}\right)_{1,2} \mp \operatorname{tg}\alpha\left(\frac{d\beta}{dl}\right)_{1,2} - \operatorname{tg}^2\alpha\left[\frac{\omega^2 r^2 \sin\sigma}{a^2} + \frac{1}{a^2}\left(\frac{dl}{dl}\right) + \frac{1}{\tau}\left(\frac{d\tau}{dl}\right)\right.$$

$$\left. + \frac{\lambda_{2,1}\sin\sigma\cos\beta}{r(\lambda_{2,1}\cos\beta - \sin\beta)} + \frac{1}{J}\frac{N\cos\beta - M\sin\beta}{\lambda_{2,1}\cos\beta - \sin\beta}\right] = 0$$

In these relationships

$$\alpha = \sin^{-1}(1/M) \quad J = 1 - (W_l/a)^2 \quad K = -W_l W_\varphi/a^2$$

$$L = 1 - (W_\varphi/a)^2 \quad M = \frac{1}{a^2}\left[\left(\omega^2 r + \frac{W_l^2}{r}\right)\sin\sigma + \frac{a^2}{\tau}\frac{d\tau}{dl} + \frac{\partial l}{\partial l}\right]$$

$$N = [1 - (W/a)^2]\left[(W_\varphi/r + 2\omega)\frac{\sin\sigma}{W_l} + \frac{1}{W_l^2}\left(\frac{1}{r}\frac{\partial l}{\partial\varphi} - \frac{T}{r}\frac{\partial s}{\partial\varphi}\right)\right] + \frac{1}{a^2 r}\frac{\partial l}{\partial\varphi}$$

Based on these equations, starting out from an initial line which is outside of the sonic line of the detached wave involved, and on the basis of the corresponding boundary conditions, it is possible to solve for the supersonic intake flow field.

We know that when the speed which corresponds to intake is supersonic and the meridional component of it is subsonic, it is possible for the disturbances produced in the blades to spread in the direction of the upper reaches of the flow. Because of this, in front of the blade cascade one sees set up a condition of stable periodicity. In this way, using the characteristic curve method, beginning from the assumption of a semi-infinite blade cascade, we went through the calculations involved for three or four passageways. In these flow fields the M numbers and the β values for the corresponding positions were all the same and satisfied the periodicity conditions. Moreover, when we included in the range a place which

was infinitely distant from the blade cascade, the tangential distance was one cascade length and this type of control body was set up as the basis for the basic aerodynamic and thermodynamic equations necessary in order to solve for even and uniform conditions of incoming flow. After carrying out quite a number of this type of calculations, it became possible to precisely determine unique angles of intake. From this, it is not difficult to obtain blade forms which satisfy unique angle of attack relationships and at the same time, we also solved for the flow field of the supersonic intake area.

3. PASSAGEWAY SHOCK WAVES

Normally, passageway shock waves are extensions of shock waves in front of the blade cascade in the direction of blade cascade passageways inside. As far as such conditions of these passageway shock waves as position, configuration and strength are concerned, we have carried out a good deal of experimental research in this area. On the basis of the results in [3,4], generally speaking, what appears in the inside of passageways are oblique shock waves.

In order to accurately analyze the situation in which we find the gas flow in front of and behind the shock wave being considered, strictly speaking, because of the qualities of space involved, one should make use of the shock wave relationships presented in [7]. In order to obtain formulae for expressing problems that are easy to explain, this article still makes use of simple relationships of the planar oblique type.

As far as planar oblique shock waves are concerned, there are two types of different situations. One of these is the oblique shock wave in which $\beta_2 = \beta_1 - \varepsilon$ is the case (Figure 1). Besides this, ε is the angle of folding for the corresponding air flow. It is determined from the air flow parameters for the area in front of the waves concerned, and is

$$\operatorname{ctg}\varepsilon = \frac{M_1^2 \sin^2\mu_1}{(1-\lambda^2)(M_1^2\sin^2\mu_1 - 1)} - \operatorname{tg}\mu_1 \qquad (1)$$

In this equation $\lambda^2 = (k-1)/(k+1)$. μ_1 represents the included angle between the incoming flow and the shock wave involved.

After going through the shock wave, the magnitude of the speed of the gas flow also exhibits changes, that is

$$\frac{W_2}{W_1} = \frac{M_2}{M_1}\frac{a_2}{a_1} = \frac{1+\lambda^2(M_1^2\sin^2\mu_1 - 1)}{M_1^2 \sin\mu_1 \sin\mu_2}$$

From the velocity triangle which is shown in Figure 1, one can see that when going through shock waves, changes in the numerical values for the speeds of the corresponding gases as well as in their direction of flow cause changes in the absolute numerical velocity values for these gases as well as in their directions, and one can see the production of jumps in the tangential components concerned. From the figure one can learn that

$$\begin{aligned}\Delta(V_\theta r) &= r(W_1\sin\beta_1 - W_2\sin\beta_2) \\ &= rW_1\sin\beta_1\left[1 - \frac{\sin\beta_2}{\sin\beta_1}\frac{1+\lambda^2(M_1^2\sin^2\mu_1 - 1)}{M_1^2\sin\mu_1\sin\mu_2}\right] \\ &= 2rW_1\sin\beta_1(1+\operatorname{ctg}\beta_1\operatorname{ctg}\mu_1)(\sin^2\mu_1 - 1/M_1^2)/(k+1)\end{aligned} \qquad (2)$$

From these equations, one can see that the jumps in the velocity moment of the gas flow being considered, $\Delta(V_\theta r)$ and M_1, μ_1 are related to β_1. Most particularly in the case of the positive shock wave in the illustration, $\mu_1 = \pi/2, \beta_1 = \beta_2 = \beta$, and on this basis, we can obtain

$$\Delta(V_\theta r) = 2rW_1\sin\beta(1 - 1/M_1^2)/(k+1) \qquad (3)$$

When passing through this positive shock wave, even though the corresponding gas flow does not give rise to bending, due to jumps in the numerical values for the velocities involved, it does give rise to jumps in the value of $\Delta(V_\theta r)$.

Another type of situation is the one shown in Figure 2, that is, $\beta_2 = \beta_1 + \varepsilon$. In such a situation, $\Delta(V_{\theta r})$ is similarly related to M_1, μ_1 and β_1, that is

$$\Delta(V_{\theta r}) = 2rW_1 \sin\beta_1(1 - \operatorname{ctg}\beta_1 \operatorname{ctg}\mu_1)(\sin^2\mu_1 - 1/M_1^2)/(k+1) \tag{4}$$

What we are primarily concerned with in this type of situation as far as the orthogonal shock wave is concerned, is the simplification of (4) into (3).

As far as these two types of oblique shock waves are concerned, the absolute total pressure ratios of the gas flow in front of the wave and the gas flow behind the wave can both be represented as

$$\frac{P_{20}}{P_{10}} = (k+1)^{\frac{k+1}{k-1}}\left(\frac{1}{2kM_1^2\sin^2\mu_1 - k + 1}\right)^{\frac{1}{k-1}} \times \left\{\frac{M_1^2\sin^2\mu_1\left[1 + \frac{k-1}{k}\frac{\omega}{RT_{10}}\cdot\Delta(V_{\theta r})\right]}{(k-1)M_1^2\sin^2\mu_1 + 2}\right\}^{\frac{k}{k-1}} \tag{5}$$

In this equation, the quantity $\Delta(V_{\theta r})$ can be calculated by dividing up the task between Equations (2) and (4).

It can be seen that the larger the M number in front of the wave is, the larger $\Delta(V_{\theta r})$ is, and the larger the ratio of total absolute pressures P_{20}/P_{10} is.

If we make use of the corresponding total pressure ratio of gas flows in order to represent losses produced after going through an oblique shock wave, then it is possible to write

$$\frac{P'_{20}}{P'_{10}} = (k+1)^{\frac{k+1}{k-1}}\left(\frac{1}{2kM_1^2\sin^2\mu_1 - k + 1}\right)^{\frac{1}{k-1}}\left[\frac{M_1^2\sin^2\mu_1}{(k-1)M_1^2\sin^2\mu_1 + 2}\right]^{\frac{k}{k-1}} \tag{6}$$

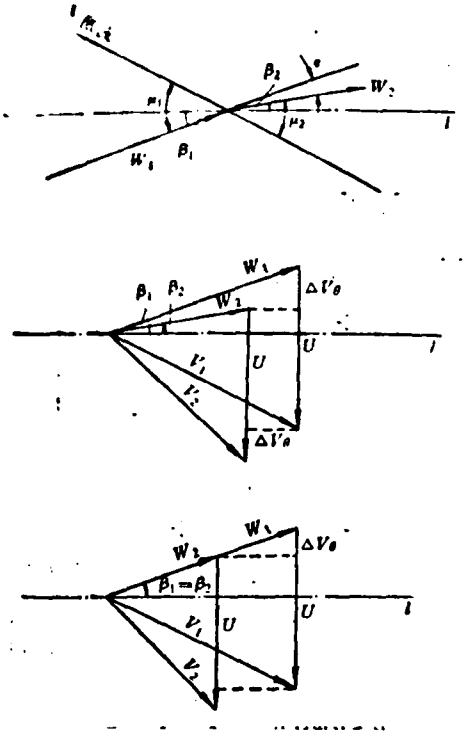

Figure 1. The oblique shock wave $\beta_2=\beta_1-\varepsilon$ and the velocity triangle for the gas flow both in front of and behind the wave
Key: 1--shock wave

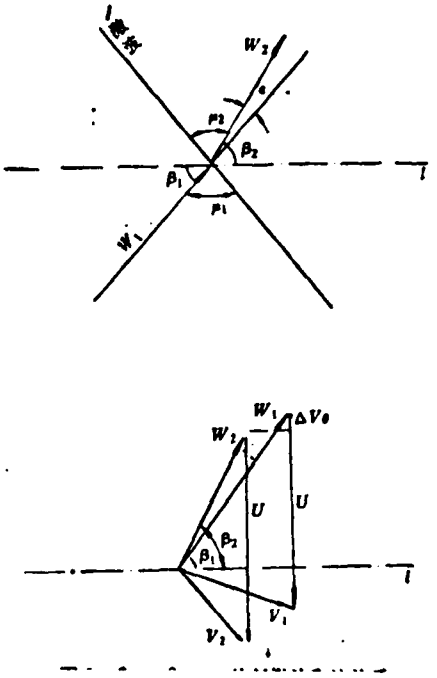

Figure 2. The oblique shock wave $\beta_2=\beta_1+\varepsilon$ and the velocity triangle for the gas flow both in front of and behind the wave

One obvious characteristic of this equation is that the losses are only determined by $M_1 \sin \mu_1$, and are not related to β_1. In this way, we are easily capable of going through aerodynamic designs in order to produce different kinds of shock wave systems so that the losses produced are relatively small and $\Delta(V_{\theta r})$ is relatively large. Of course, the losses we are talking about here are still losses which are produced by going through the body of a shock wave itself. However, it can be hoped that the separation losses which are caused by shock waves which are relatively weak will also be relatively small.

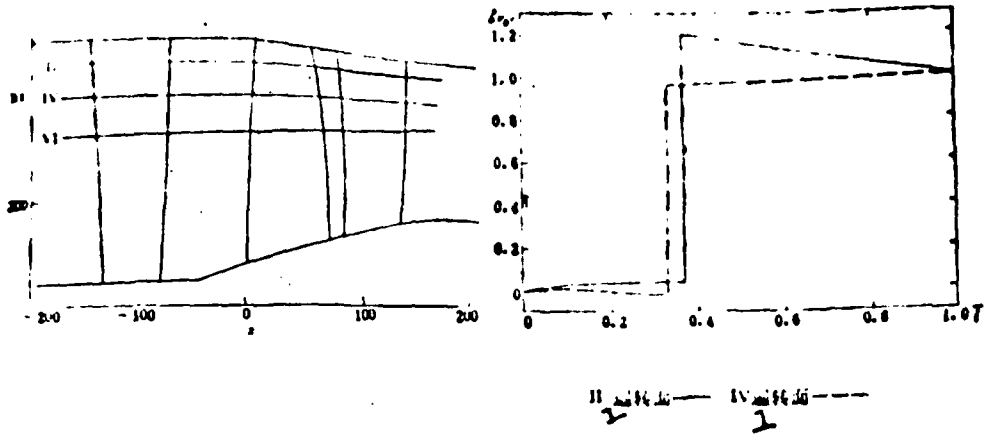

Figure 3. Flow Path Diagram

Figure 4. Distribution of $\bar{v}_{\theta r}$ Along the Passage Centerline on Surface of Revolution
1 - surface

From (5) and (6), it is possible to obtain the relationship set out below which connects the absolute total pressure ratios for gases in front of and behind a shock wave to the corresponding total pressure ratios, that is

$$\frac{P_{20}}{P_{10}} = \frac{P'_{10}}{P'_{10}}\left[1 + \frac{k-1}{k}\frac{\omega}{RT_{10}}\Delta(V_{\theta r})\right]$$

What is interesting is the fact that even though $P'_{10}/P'_{10} < 1$, $P_{20}/P_{10} > 1$ is still the case.

4. CALCULATION RESULTS AND DISCUSSIONS

Concerning the use of the characteristic curve method in the intake area, one postulates a position and configuration for a passageway shock wave and then makes use of a unique flow assumption which takes into consideration the flow thickness and losses involved and applies this to the gas flow behind the wave. Concerning the carrying out of calculations of the II cross-sections and IV cross-sections of the tips of the rotors from [2], that is

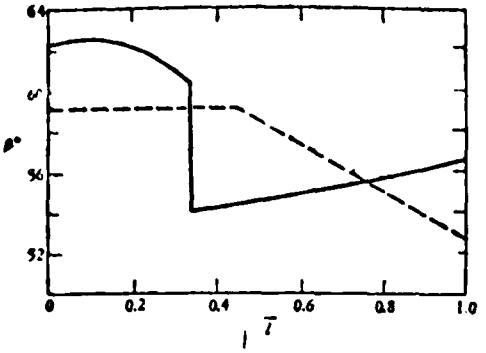

图5 II通转面气流角沿通道中线的变化
中弧线——— 计算结果——
1 2

Figure 5. Changes in the II surface of revolution gas flow angle along the center line of a passageway.

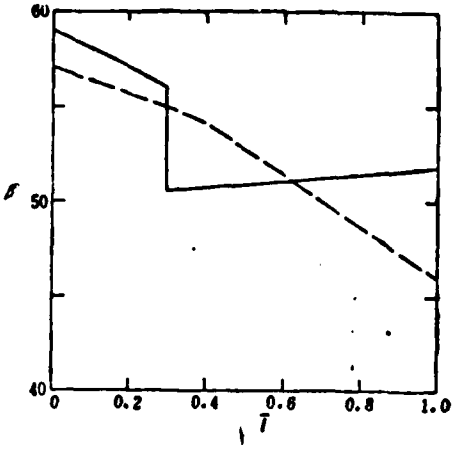

图6 IV通转面气流角沿通道中线的变化
中弧线——— 计算结果——
1 2

Figure 6. Changes in the IV surface of revolution gas flow angle along the center line of a passageway.

Key: 1--center arc line;
2--calculated result

Figure 3, we will take the results from these calculations and put them together with the calculation results derived for the subsonic surface of revolution and then take them both and move them into the center of the flow surface S_2, that is (S_{2k}) . Then, we will carry out a new set of calculations.

Figure 4 is a representation of changes in the surface of revolution II and IV along a passage centerline $V_{\theta r}$. Figures 5 and 6 are respectively the changes in the gas flow angles along the center lines of passageways which correspond these two surfaces of revolution. The important point is this. The $V_{\theta r}$ value for air flows which pass through shock waves steeply and violently increases. For the intake cross-section IV with a relatively low M number, $\Delta(V_{\theta r})$ reaches 99% of the $\Delta(V_{\theta r})$ value for the entire blade cascade passageway involved. In the case of cross-section II, in which $V_{\theta r}$ exceeds the numerical value in the exhaust, causing the air flow along the center line of the passageway behind the wave to accelerate, we see the occurrence of a turbine situation in which $V_{\theta r}$ again gradually decreases until it reaches the exhaust value. Correspondingly, when passing through an oblique shock wave, the

TABLE 1. A comparison of the results from various different methods used for calculating the II cross-section

1项目 / 2计算方法		$M_{出}$ 7	$M_{出}$ 8	$(Vor)_{出}$ 9	$(Vor)_{出}$ 10	$(\Delta s/R)_{出}$ 11	$\Delta(Vor)_{出}$	$M_{出}$ 12
3二元分析	4正激波	1.397	0.711	−3.91	48.0	0.0585	46.7	0.766
	5斜激波	1.130	0.778	−1.91	51.7	0.0621	47.9	0.752
6特征线斜激波		1.321	0.815	1.10	45.8	0.0230	38.5	0.864
$S_{进}$		M_{∞}	1.301	$\Delta(Vor)_{总}$ 13	57.6		$M_{出}$ 12	0.871

Key: 1--quantity; 2--calculation method; 3--two-dimensional analysis; 4--orthogonal shock wave; 5--oblique shock wave; 6--characteristic curve oblique shock wave; 7--front; 8--behind; 9--front; 10--behind; 11--wave; 12--exhaust; 13--total

corresponding angle of air flow along the center line of the passageway involved drops abruptly. In the IV cross-section, these values are somewhat higher than the numerical values in the exhaust; moreover, in the II cross-section, they are somewhat lower than the numerical values in the exhaust section; in the passageways that follow, these values gradually come back up and reach the values which are found in the exhaust. Obviously, if the shock wave concerned is an orthogonal one, then the gas flow angle behind the wave will not change.

What is worthy of note is the fact that after we make use of the oblique shock wave model in each of the various cross-sections in the exhaust area, when power is added up and the calculation of the inverse problem in S_2 is calculated, the numerical values which one gets are relatively close to each other, the error being inside a range of 3%. When we make use of two-dimensional analysis of shock waves in our calculations, this error is very large (Tables 1 and 2). This shows the fact that the oblique shock wave model is capable of giving excellent results and the reason for this is that it molds itself relatively more closely to the actual situation of the shock waves in the vicinity of the center lines in the passageways

TABLE 2. A comparison of the calculated results obtained by the use of different methods for cross-section IV.

1 项 目 / 2 计算方法		$M_{出}^{7}$	$M_{出}^{8}$	$(Vor)_{出}^{7}$	$(Vor)_{出}^{8}$	$(\Delta_1/K)_{出}^{9}$	$\Delta(Vor)_{出}^{10}$	$M_{出}^{10}$
3 二维分析	4 正激波	1.373	0.751	−4.83	37.0	0.0360	39.1	0.760
	5 斜激波	1.385	0.783	−5.08	39.9	0.0379	38.6	0.767
6 特征线斜激波		1.307	0.837	−1.29	35.1	0.0171	37.0	0.790
S_{1c}		M_{∞} 1.216			$\Delta(Vor)_{出}^{11}$ 36.2		$M_{出}^{10}$ 0.798	

Key: 1--quantity; 2--calculation method; 3--two-dimensional analysis; 4--orthogonal shock wave; 5--oblique shock wave; 6--characteristic curve oblique shock wave; 7--front; 8--behind; 9--wave; 10--exhaust; 11--total

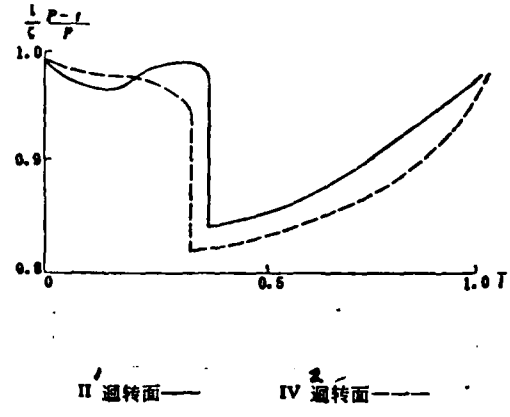

Figure 7. The distribution of the surface of revolution $\frac{1}{\zeta}\frac{P-t}{P}$ along the center line of the passageway involved.

Key: 1--surface of revolution II
2--surface of revolution IV

of the blade cascades being studied. The main reason is also as follows: On the center line of the passageways involved, the gas flow behind the shock waves concerned is in a turbine configuration; however, this does not mean that the entire passageway is necessarily in the same condition. In fact, in these passageways, the various configurations and strengths of shock waves are extremely different from each other. Because of this fact, generally speaking, in order to accurately solve this type of flow, one ought to do the sort of thing pointed out in [7] that is to say, make simultaneous calculations of several S_1 flow surfaces and several S_2 flow surfaces.

From Figure 4, it can also be seen that, even though the intake M number of the II cross-section is relatively high, it is only necessary to design the structure in an appropriate way and it becomes possible for the M number in front of the oblique shock wave concerned to not be excessively high for the losses of this type to remain small and for one to obtain the required total pressure ratios.

Figure 7 is a display of the changes in $(P-\varepsilon)/\zeta P$ for cross-sections II and IV along the center line. This Figure points out that this parameter, when it passes through an oblique shock wave also produces abrupt changes in its values. This interesting result clearly points out the fact that the flow filament S_2 behind the shock wave concerned gives rise to deflections.

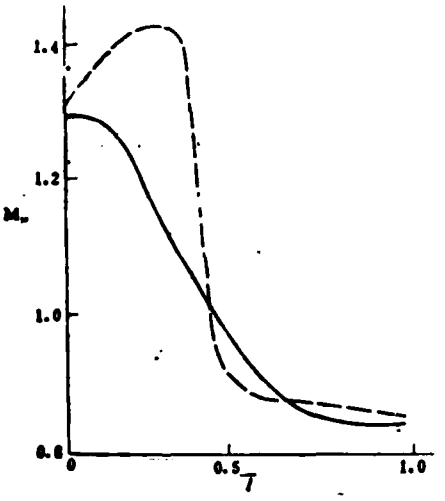

S_{2c} - - - -; Normal Calculation of S_2 Flow ——

Figure 8. A comparison of the calculated standard through current for the surface of revolution II and S_{2c} calculated Mach number.

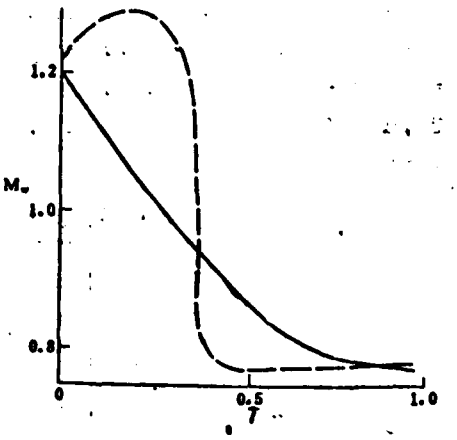

S_{2c} - - - - -

Normal Calculation of the S_2 Flow ——

Figure 9. A comparison of the standard calculated through flow for the surface of revolution IV and the calculated S_{2c} Mach number.

Finally, Figures 8 and 9 present the corresponding distributions of M numbers which are obtained for cross-sections II and IV by making use of calculations of the standard through flow and calculations of the S_{2c} which takes into consideration oblique shock waves. It is possible to see that in the interval between the front and the back of the outside of blades, the errors in these two quantities are not large. However, inside the blades the two quantities are quite distinct from each other. This is particularly true in the area which is in the vicinity of the shock wave. In front of the wave, the M number which is calculated on the basis of the standard method is much smaller when compared to its companion quantity.

Behind the wave, it will be larger than its companion quantity. It can be seen from this that in order to cause the air flow calculations for a transonic compressor as well as its design closely match the actual situation, it is necessary to make use of the distributions of the quantities $V_{\theta r}$, S and $(P-\rho)/\zeta P$ as they were calculated with due consideration given to the shock waves involved, and use these distributions to transfer into the calculation of S_{2c}. Moreover, looking from the point of view of our calculations, in the area in the vicinity of the shock waves involved, the S_{2c} calculation stations ought to be selected in larger numbers. In this way, the calculations for the area in the vicinity of the shock wave would become even more accurate.

5. CONCLUSIONS

Passing through a shock wave, the numerical values of velocities which correspond to gases under consideration as well as the direction of movement of these gases exhibit changes. These changes lead to changes in the absolute numerical values for velocity and direction of movement as these relate to the same gases. Because of these factors, one sees the occurrence of jumps in the tangential

velocities, and these jumps produce strong and violent compression effects on the gases involved.

The results of calculations show that on the center lines of passageways there are abrupt drops in the gas flow angles which correspond to the passage through the shock wave or waves involved. These angles of flow are sometimes lower than the angles of flow at the exhaust. Moreover, $\Delta(V_{\theta r})$ exhibits sudden increases, even to the point where it is possible for its values to exceed the values found at the exhaust. The numerical values of $V_{\theta r}$ at the exhaust and the values which come out of calculations of S_{2c} vary from each other in a range of about 3%. At the same time, the results of calculations of $(P-t)/\zeta P$ point out that when passing through a shock wave, the flow surfaces exhibit deflection and twisting. This is an important point.

Concerning the taking of the results of calculating the surface of revolution by using this type of oblique shock wave model and substituting them into the calculations of S_{2c}, the distribution of parameters which one obtains in this way exhibit very large differences from the amounts of flow calculated as standard conditions and those present on the inside of the blades. This discrepancy is particularly pronounced for values calculated in the areas in front of shock waves and values calculated for areas behind them.

REFERENCES

[1] Wu Chung-hua: A General Theory of Three-Dimensional Flow in Subsonic and Supersonic Turbomachines of Axial, Radial, and Mixed Flow Types, *ASME Paper 50-A-79* (1950); Trans. *ASME*, NOV. (1952) or *NACA TN 2604*, (1952).

[2] Academia Sinica: Shen Yang Aviation Engine Company; Methods and Applications of the Design Theory of Three-Dimensional Flow in Transonic Axial Type Compressors, Engineering Thermal Physics Report, 1, 1, (1980), 44.

[3] Dunker R. J., et al.: Experimental Study of the Flow Field Within a Transonic Axial Compressor Rotor by Laser Velocimetry and Comparison with Through-Flow Calculations, *J. of Engineering for Power*, 100, Apr. (1978).

[4] Dunker R. J. and Hungenberg H. G.: Study of the Flow Field behind a Transonic Axial Compressor Rotor using Laser-Anemometry and Unsteady Pressure Measurements, Proceedings of 4 th ISABE, (1979).

[5] Moeckel W. E.: Approximate Method for Predicting Form and Location of Detached Shock Waves Ahead of Plane and Axially Symmetric Bodies, *NACA TN 1921*, (1949).

[6] Wu Chung-hua and Costilow E. L.: A Method of Solving the Direct and Inverse Problem of Supersonic Flow along Arbitrary Stream Filaments of Revolution in Turbomachines, *NACA TN 2492*, (1951).

[7] Xu Jian Zhong: Shock Wave Relationships in Turbine Wheel Mechanisms, Mechanical Engineering Report, 16, 3, (1980)

AN THEORETICAL ANALYSIS ON THE STREAM SURFACE OF REVOLUTION WITH SUPERSONIC INLET FLOW IN A TRANSONIC AXIAL COMPRESSOR

Xu Jian-zhong Jiang Zuo-ren Yang Jin-sheng Zhang Ying
Du Zhuan-she
(Institute of Engineering Thermophysics, Academia Sinica)

Abstract

Starting from jumps of absolute velocity and its tangential component due to changes of magnitude and direction of the relative velocity while passing through a shock and using the relations for a plane oblique shock, the expressions for $\Delta(V_u r)$ loss and total pressure ratio of gas are derived and the fact that the gas is supercharged across the shock is explained theoretically. An aerothermodynamic analysis on the stream surface of revolution with supersonic inlet flow is made by assuming the location and shape of the passage shock and applying the characteristics method in the inlet region. Some of important features in a transonic compressor can be seen from the analysis. The moment of velocity from such calculations is close to that given in the calculation of inverse problem along a central S_2 stream surface. There are great differences in Mach number distributions between the calculations of the central S_2 stream surface with the variations of $V_u r$-$\Delta s/R$ and the streamfilament thickness in which the shock relations are taken into account as its input, and of the conventional average S_2 stream surface.

PRELIMINARY RESEARCH ON ABLATION EXPERIMENT TECHNIQUES IN TURBULENT FLOW OVER A FLAT PLATE SPECIMEN*

Han Yin-da, Wang Ke-xiang, Yu Guang-rong
Chinese Aerodynamic Research and Development Center (CARDC))

SUMMARY

This article involves the test production of a new type of method involving an electric arc heated supersonic flow placed at a small angle to a flat plate specimen. This type of method is capable of overcoming the inadequacies of the pipe test method which is employed now. The speed of ablation which is measured in this method is relatively uniform. Moreover, it is capable of easily measuring the surface temperature and surface radiant heat flow. Also in this article there is a discussion of experimental principles, the structure of experimental equipment, measurement parameters and calculation methods. This study was completed in a measurement arc chamber in which pressures ranged from 10.2 to 17.3 kg/cm^2 and enthalpies of from 520 to 2440 kcal/kg. This article gives the results of ablation experiments with teflon models under five types of turbulent conditions.

*This article was read at the 2nd Annual All-China Engineering Thermal Physics Conference in Hang Zhou in November of 1978.

SYMBOLS

a : sonic speed; enthalpic loss coefficient behind the throat section of a jet tube

G_a: air flow amount

G_w: amount of cooling water flow

H_o: total enthalpy

H_r: recovery enthalpy

h : static enthalpy

L : material specimen model thickness

n : number of measurements taken

P_o: total pressure

p : static pressure

q : heat flow

s : entropy

T : temperature

u : speed of gas flow

$\overline{V}_t$: average curve ablation speed

x : length beginning from the extension section entrance

ρ : density

μ : viscosity coefficient

α : air constituent

τ : shear stress

ε: full radiation coefficient

σ : Boltzmann constant

Superscripts:

* : reference enthalpy condition

/ : wave interference condition

Subscripts:

cw: cooled wall

e : outside edge of boundary layer

ex: jet tube exhaust

R : radiation

w : heated wall; ablation surface

x : along the direction of the flow line

* : throat passage

∞ : room conditions

1,2: before ablation and after ablation or measurement points

1. FOREWORD

When a satellite, a spacecraft or any such high speed aircraft re-enters the atmosphere it is going to meet with extremely high aerodynamic heating. Because of this, when the various types of high speed aircraft are designed, it is necessary to carry out heat protection calculations. Experiments carried out on the surface in order to simulate material ablation confirm the theory of the calculations, give precise determinations of the ablation performance of materials as well as providing an important foundation for heat protective designs and effective measures to this end. In the re-entry process of spacecraft and aircraft, areas of turbulence cover the greater part of the surface of the aircraft. Because of

this, the study of ablation under turbulence flow conditions is not only absolutely necessary; moreover, the data which is offered by experiments in turbulence flow ablation has a very large influence on heat protective designs.

At the beginning, people used pipe type equipment in order to carry out research experiments in turbulence flow ablation [1]. Figure 1 shows the flow field for a re-entry nose cone with a cone shape. Let us assume that AB and CD flow lines define the range around the outside of the boundary layers of the object in which it is possible to ignore the enthalpic gradient. These flow lines on the front surface of a shock wave define the limits of a ring belt of which the radius is R_s. We recognize the fact that the flow in the ring belt on the front circumference ABCD of the nose cone is an equienthalpic expansion flow and this flow will on the surface of the object produce stagnation point conditions at P_o and H_o. From this condition, people's thinking led to the idea of using a jet tube with radius R_s to replace the radius R_s flow tube. This would offer stagnation chamber conditions at P_o and H_o, and one could use the jet tube flow to reproduce the equienthalpic expansion flow around the nose cone of the spacecraft. Both inside China and abroad, research workers employed pipe type equipment in the performance of large amounts of experimental research [2,3]. However, the pipe technique possesses certain inherent drawbacks. The most important of these are the following. If one uses this type of equipment, observation is inconvenient along with the fact that, in the ablation process, if one increases the diameter of the tube, the heat flow drops and it is difficult to determine precise values for this kind of unstable effect. In order to overcome these shortcomings, workers in the field carried out research in the area of the experimental technology involved with turbulent flow flat plate ablation.

2. BASIC PRINCIPLES AND THE STRUCTURE OF EXPERIMENTAL EQUIPMENT

Concerning the high temperature air flow which is shot out from the electric arc heating apparatus, when it passes through the extension section it forms laminar flow boundary layers and in the vicinity of the throat passage of the jet tube, it turns into a turbulence boundary layer flow. At the place where there is an exhaust in the wall of the rectangular supersonic two-dimensional jet tube, there is positioned a piece of equipment of the one-flat-plate-model-type which is set at a certain fixed angle of attack to the air flow; these two are fitted so closely together that there is no gap between them (see Figure 2). The boundary layers which are on this model are natural extensions of the boundary layers on the surfaces of the walls in the jet tube. From these, on the flat plate model, one obtains a fully developed turbulent flow boundary layer and because of the action of the back pressure gradient which is formed due to the oblique shock wave of the forward edge of the flat plate model, one sees an increase in the simulation range of parameters in the model.

Ablation is an extremely complex process. It is a phenomenon which is the result of the combined actions of such various factors as thermal energy exchange between air flows, pressure, shear, chemical reactions and so on. In the ablation process, the related parameters can be described using the equations set out below:

$$P_0(\text{或}p) \tag{1}$$

$$\alpha_i = f(P_0, H_0) \qquad i^2\text{为 } O, N, NO \text{ 等} \tag{2}$$

$$q_{cw} = 0.0296\rho^* u_e (P_r^*)^{-2/3} (\mathrm{Re}_x^*)^{-1/5} (H_r - h_{cw}) \tag{3}$$

$$\tau = 0.825 q_{cw} u_e (H_r - h_{cw}) \tag{4}$$

1- or 2- is 3- etc.

The physical parameters ρ^*, μ^* as well as other similar parameters are determined by the equation below with reference to enthalpy and on the basis of calculations concerned with enthalpy, that is

$$H^* = 0.22H_0 + 0.5h_{cw} + 0.28h_e \tag{5}$$

The effective heat of ablation is an important parameter to the evaluation of the heat resistant performance of ablation materials. This parameter represents the amount of heat which a unit of mass of an ablation material is capable of absorbing or blocking and its definition is as follows:

$$H_{eff} = [\dot{q}_{cw}(H - h_w)/(H_0 - h_{cw}) - \varepsilon\sigma T_w^4]/\rho\bar{V}_1 \qquad (6)$$

From the various equations set out above, the only independent parameters there are P_o or (p), H_o and u_c. When one is dealing with a situation in which the dimensions and configuration of a re-entry body are determined, then the three parameters P_o or (p), H_o and u_c are only determined by re-entry speed (or M) and the re-entry altitude. Because of this, in these experiments, the simulation of the three parameters P_o or (p), H_o and u_c, is simply based on the reconstruction of the re-entry ablation environment. To summarize what was said above, in turbulent flow flat plate ablation experiments, the main parameters which must be measured are H_o, P_o (or p), $\dot{q}_{cw}$, $\bar{V}_1$, T_w and ε as well as other related parameters.

The complete array of experimental equipment includes an electric arc heating device, an induction section, an extension section and rectangular form jet tube, model and measuring device, supports, water vapor and its control system as well as various types of testing systems and other related gear. The various types of components involved were designed and manufactured on the basis of such principles as the assumption that the power from the electric arc in the electric arc heating device, its operational configuration and the oblique shock wave which is produced by the maintenance of the front edge of the flat plate model and the expansion wave which is reflected back when the oblique shock wave meets the free boundary do not fall on the model. In the case of the jet tube, a simple form of analysis is employed and we make use of computers to carry out the surface coordinate calculations. The model and the jet tube involved have the same width. The measuring

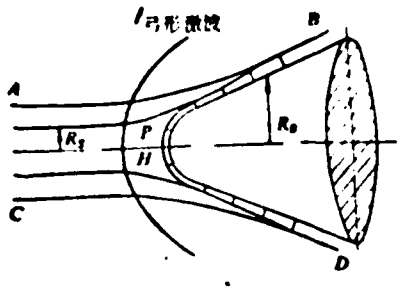

Figure 1. Spherical-conical re-entry nose cone flow field.
Key: 1--bow-shaped shock wave

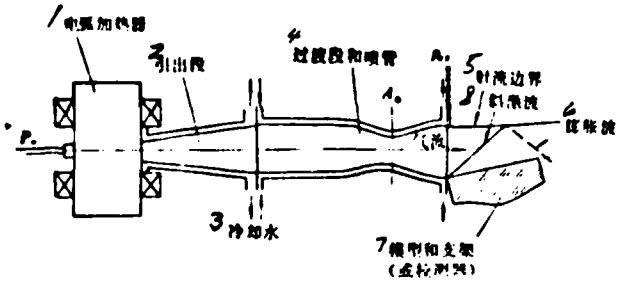

Figure 2. Principles behind the experimental equipment.
Key: 1--electric arc heating device; 2--induction section; 3--cooling water; 4--extension section; 5--jet boundary; 6--expansion wave; 7--model and support (or testing device); 8--oblique shock wave

devices and the ablation samples have heat absorbing surfaces with the same dimensions. The most important among these are the heat sink type flat plate pressure distribution measuring device (see Plate 2(a)) and the heat flow distribution flat plate measuring device (see Plate 2(b)) which are used to make precise measurements of the ablation environment of the sample models. The supports are used to hold the models and the measuring devices. During these experiments, the angle of deflection which was chosen for the flow over the models was 10°.

3. PARAMETER MEASUREMENTS AND CALCULATIONS

In order to obtain an ideally uniform flow field, it is necessary during adjustments to the configurations to maintain the jet tube exhaust static pressure at a value which is basically equal to the pressure of the surrounding environment. Once the adjustments have been made, it is also necessary to make use of the experimental configurations set out in Table 1. In these experiments, we made use of principles which are essentially the same as those which were presented by Winovich in his total pressure

flow amount method [4], in order to determine precise values for the total enthalpy H_0 in the throat portion of the jet tubes being considered. When the amounts of flow are maintained precisely unchanged under conditions of hot and cold (by the use of an installed jet nozzle speed control), one makes use of a cold air standard to precisely determine the effective area of the throat passage, that is

$$A_{*eff} = G_a\sqrt{T_{*}}/396.5P_0 \qquad (7)$$

We made use of a turbine wheel flow amount meter and a heat sensitive electrical resistance temperature gauge in order to make repeated measurements of the amounts of flow of the jet tube cooling water and the rise in temperature associated with this water. From the energy equilibrium principle, it is possible to obtain the total enthalpy for jet tube exhausts, that is

$$H_{0x} = H_{0*} - aC_pG_W\Delta T/G_a \qquad (8)$$

TABLE 1. Experimental configuration parameter table.

1 参数 \ 3状态 / 2单位		1	2	3	4	5	6	7
4 气流总压 P_0	5 公斤/厘米²	12.4	15.1	10.4	10.2	10.5	17.1	17.3
6 喷管出口总焓 H_{0x}	7 大卡/公斤	520	997	1500	2030	2440	1336	1897
8 喷管种类	—	9 锥面喷管					10 型面喷管	

Key: 1--parameter; 2--unit; 3--configuration; 4--total gas flow pressure; 5--kg/cm²; 6--jet tube exhaust total enthalpy; 7--kcal/kg; 8--type of jet tube; 9--conical surface jet tube; 10--rectangular jet tube

We made use in these experiments of heat sink type pressure measuring flat plates and pressure change transmitting devices to measure the pressure distribution at five points on the center line of the models involved; moreover, at the same time, we took measurements of the static pressure in the jet tube exhaust. The cooling water heat equilibrium type heat measuring device (water

calorimeter) measured the cold wall heat flow at three points on the center line of the flat plate model. In order to make it easier to test produce a zero point thermal measuring device and make use of sweep measurement [5] as a substitute for fixed type measurement. We used this approach to get the heat flow distribution results which are presented here (see Table 2). During the process of ablation of a sample model we made use of an improved photoelectric colorometric high temperature measuring device to measure the colorometric temperatures on the ablation surface and we recognized the fact that the colorometric temperature $T_s \approx T_w$. We also made use of a radiation type high temperature measuring device in order to measure the radiated surface temperature of the model involved, that is T_R. On the basis of the Steven-Boltzmann principle, we can know that

$$\varepsilon = (T_R/T_w)^4 \qquad (9)$$

As far as ablation speed was concerned, we made general use of the average time method to determine it and we recognized the fact that ablation is of a quasi-fixed nature and for several models of combustion, the ablation measurements before and after the process in terms of the thickness of the models involved can be obtained from the equation below, that is

$$\bar{V}_i = 1/n \cdot \sum_{i=1}^{n} (L_{i1} - L_{i2})/t_i \qquad (10)$$

Concerning a few localized areas of ablation, if one measure the ablation in step and column and other similar types of ambient stall spots by the use of the instantaneous method of determination one can find the curve which relates the amount of ablation $\Delta\delta$ to the ablation time t; moreover, by solving for the slope of the curve at various different instants, it is possible to obtain the instantaneous speed of ablation, that is

$$V_{ti} = d(\Delta\delta)_i/dt \qquad (11)$$

Testing procedures have demonstrated that the pressure p_1 at the first measurement point on the flat plate is the static pressure behind the oblique shock involved. We already know that $\xi = p_1/p_{\infty}$, and if we select the specific heat $\kappa = 1.2$, then we get [6]

$$M_1^2 = \{M_\infty^2[(\kappa+1)\xi + (\kappa-1)] - 2(\xi^2-1)\}/\{\xi[(\kappa-1)\xi + (\kappa+1)]\} \quad (12)$$

When M_1 and p_1 are precisely determined, then we can make use of the relationships presented below, that is

$$M_1 = u_{e1}/a_1 = \sqrt{2J(H_{0\infty} - h_1)}/a_1 \quad (13)$$

$$a_1 = f_1(p_1, h_1) \quad (14)$$

By repeatedly consulting the thermodynamic function table for air [7], we managed to directly obtain a simultaneous solution for the two equations presented above. Because of this, it is possible to precisely determine all such parameters as a_1, h_1, u_{e1}, ρ_1, s_1 for the point involved. We recognize the fact that the gas flow over the flat plate is equienthalpic and because of this fact, all the parameters for the various points on the center lines of the flat plate models involved can be solved for by using the methods presented above.

TABLE 2. Typical parameter measurement results

1状态		4					6				
3参数 \ 2测点		1	2	3	4	5	1	2	3	4	5
4 压力 p_i	8公斤/厘米²	1.34	1.11	0.98	1.04	1.18	2.23	1.90	1.82	1.36	1.13
5 水卡热流 q_{w}	9卡/厘米²·秒	152		117		128	—		—		—
6 零点热流 q_{w}	9卡/厘米²·秒	124		119		123	178		134		103
7 理论热流 q_{w}	9卡/厘米²·秒	153		118		137	181		158		113

Key: 1--state; 2--measurement point; 3--parameter; 4--pressure; 5--water calorimeter heat flow; 6--zero point heat flow; 7--theoretical heat flow; 8-- kilograms per centimeter square; 9--calories per square per second.

4. ANALYSIS OF RESULTS AND DISCUSSION

1. The distinguishing characteristics of turbulent flow ablation. After going through experiments concerning three aspects of operation, we were able to distinguish the various characteristics of turbulence flow ablation. Teflon (polytetrofluoroehthylene) is an excellent ablation material. During ablation, the surface temperature of it is very low and it reacts differently to laminar and turbulent flows. Its effective ablation heat is represented by the expression:

$$H_{e,t} = q_{cw}/\rho\bar{v}_t \qquad (15)$$

Under five relatively high configurations, the ablation measurements which resulted for teflon are shown in Figure 3 and these results agree very well with the turbulence flow ablation results found in [6].

Besides this, by definition we have the fact that $Re_x = \rho u x/\mu$ and it is shown by the calculations involving the first measurement point on the flat plate, that $Re_x = 5.4 \times 10^5 - 4.2 \times 10^7$ and all these values are larger than the critical turning point for Reynolds numbers 5×10^5. We made use of formula (3) and the Eckert flat plate reference enthalpy method in order to calculate the theoretical turbulent flow heat flow distribution and the measured values agree with the corresponding theoretical values within a range of ±15%. As far as conical surface jet tubes are concerned, we made use of the equation below in order to correct wave system interference [8], that is

$$q'_{cw}/q_{cw} = (p'/p)^{0.85} \qquad (16)$$

The results of these calculations are set out in Table 2. The measured values and the theoretical values obtained on the basis of corrections for wave system interference tend to agree with each other. Their numerical values are close and the largest error involved is smaller than ±17%.

2. The influence of flow fields. Concerning the case in which the exhaust flow field of a conical surface jet tube is not sufficiently ideal, one can see from the two photographs in Plate 2c which were taken from orthogonal directions that there are both expansion and compression wave systems in existence. However, if one takes a look at the ablation results, one can see that the wave system interference has still not created obvious troughs in the sample model surfaces. This means that the wave system interference is very weak. It can be clearly seen from the measurement results in Table 2 that the surface jet tube flow fields involved show a relatively large improvement and the flow on the flat plate closely approach the characteristics of equienthalpic expansion waves.

3. Ablation measurement results. The teflon ablation measurement results are set out in Table 3. Plate 2d is a photograph of the surface situation after teflon flat plate model ablation has taken place.

TABLE 3. Measurement results for teflon ablation

1 参数 / 2 测点 / 3 状态	4 烧蚀速度 $\bar{v}_i$ 5 毫米/秒				
	1	2	3	4	5
3	0.60	0.52	0.51	0.51	0.58
4	0.68	0.64	0.59	0.56	0.58
5	0.78	0.73	0.70	0.68	0.82
6	0.74	0.71	0.66	0.64	0.63
7	0.99	0.91	0.89	0.83	0.68

Key: 1--parameter; 2--measurement point; 3--configuration; 4--ablation speed; 5--mm/sec

4. The influence of a convex base on ablation. Due to a step effect in front of a step involved, the air flow stalls and forms a stall shock wave (see Plate 2e). In the stall spots involved, heat flow and increases in stress cause local

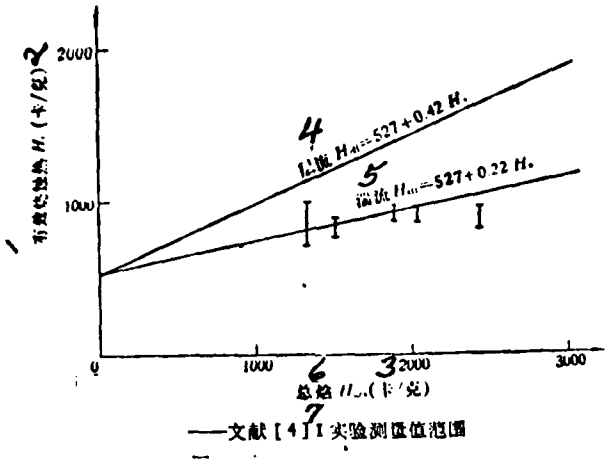

Figure 3. A comparison of teflon ablation measurement results.

Key: 1--effective ablation heat; 2--cal/gram; 3--cal/gram; 4--laminar flow; 5--turbulent flow; 6--total enthalpy; 7--range of measurement values in Experiment I in reference [4].

intensifications of ablation. However, due to the fact that in the ablation process, the steps are turned very rapidly into slopes by the combustion (see Plate 2f). If one adds to this fact a case in which the Mach number of the air flow involved is not high, then the effects of the steps are not significant and in front of the steps there is no obvious ablation trough. However, when one considers a sample going through ablation measurements without steps on the specimen, one can still get the appearance of such a trough. If one is speaking in terms of certain kinds of materials, ablation speeds in the area in front of steps can be one-and-a-half times higher than the speeds for the same samples without steps. This sort of result is in basic agreement with the results of the calculations done in [9]. The results of step model ablation have provided precious experimental data with which to further our understanding of the certain amount of sudden ambient ablation which is unavoidable with re-entering spacecraft and aircraft.

Concerning the employing of the technology of turbulent flow flat plate ablation experimentation, there has been research done in the analysis of various other aspects of the subject, such as

carbon layers, heat decomposition layer thicknesses and the nature of these layers, the way in which surface happens and the phenomena involved, insulating properties, the presence of mechanical erosion and the factors influencing it, the good points and bad points involved in the working of different types of materials as well as other questions of a similar type. However, these matters will not be discussed here.

5. CONCLUSION

The turbulent flow flat plate ablation experimentation technology has overcome the limitations of the pipe type methods. This technology is capable of quite adequately simulating the supersonic turbulent flow ablation environment present on spacecraft and aircraft which are re-entering the atmosphere and in doing this, has promoted research into the experimental technology related to turbulent flow ablation. Such experimentation proves that this type of technology is an effective means of running tests on materials which are heat resistant in terms of turbulent flow ablation and this sort of technique expands the range of experimental tasks which can be undertaken by electric arc heating devices.

What finally needs to be pointed out is the fact that the work involved in such tasks as the measuring of enthalpy by the total pressure flow amount method, the zero point measurement of heat flow as well as of surface temperature, the measurement of radiant temperature and so on, was completed by Wu Zong-sen, Li Ding-wan, Huang Yi, Gu Shi-jie and other comrades, and I wish to express thanks for this help.

REFERENCES

[1] Rose, P. H. & Offenhartz E.: Ablation Measurement in Turbulent Flow *AD-270620*, (1959).

[2] Robert E. Sheldahl and George, F. Wreght Jr: A Channel Mest Derice For Arc jet Material Ablation Studies, *AIAA 71-260*.

[3] Barry J. Mitchel: Ablative Material Tests Under Transient Heating Simulating Ballistic Reentry, *AIAA Paper 69-150*.

[4] Wilkovich, W.: On The Equilibrium Sonic-Flow Method For Evaluating Electric Arc Air Heater Performance, *NASA TND-2152*, March 1964.

[5] Kennedy, W. S., et al.: Heat Flux Measurement Using Swept Null Point Calorimentry, *AIAA Paper 71-428*, April 1971.

[6] E. H. Combort: Ablation Measurements in Turbulent Flow, *AIAA 70-226*.

[7] А. С. Плешанов, Е. В. Самуйлов, И. Б. Рождественский: Таблицы Термодинамических Функций Воздуха, Вычислительный Центр АН СССР, Москва—1962.

[8] D. E. Nestler: Pitfalls of Extrapolating Ground Test Data To Hypersonic Re-entry Conditions, *AIAA 9 th. Aerodynamic Testing Conference*.

[9] D. E. Nestler., et al.: Heat Transfer To Ste and Cavities in Hypersonic Turbulent Flow, *AIAA Paper 68-673*.

A PRIMARY RESEARCH ON ABLATION EXPERIMENT TECHNIQUE OF THE TURBULENT FLOW OVER A FLAT PLATE SPECIMEN

Han Yin-da Wang Ke-xiang Yu Guang-rong

(Chinese Aerodynamic Research and Development Center (CARDC))

Abstract

A new method utlizing a flat plate specimen placed at a small angle to a supersonic arc heated flow has been developed. This method can surmount the disadvantages of the usual pipe test method. Its observable recession rate is relatively uniform, and surface temperature and radiant heat flux can be easily performed.

This paper presents the experiment principles, the configuration of the facility, measurement and theoretical calculating method of the parameters. The study was accomplished with measured reservoir pressures ranging from 10.2 to 17.3 kg/cm^2 and total enthalpies from 520 to 2440 kcal/kg. Under five turbulent conditions the ablation test results of teflon models were given in this paper.

A NEW METHOD OF COOLING TURBINE VANES*

Gu Wei-zao, Zhang Yu-ming and Xu Hong-kun
(Institute of Engineering Thermophysics, Academia Sinica)

As far as current, state-of-the-art turbine blades in aviation engines are concerned, the generally employed cooling method is a complex one involving blast, convection and gas films; in these same advanced blades, the complexity of the construction is getting more and more extreme and the amounts of cooling gas involved is getting larger and larger. In order to raise still further the intake temperatures of turbines, it is necessary for one to look for a new way of handling cooling. This article suggests the employment of an internal cooling process within strengthened blades along with the employment of additives to lessen the transfer of heat to the blades from the fuel gases. The combination of these two measures would improve cooling. In the article below, the authors deal respectively with the bases for these measures and the temperature calculations involved with regard to the first stage guide vanes of the MK202 engine.

1. COARSENESS STRENGTHENED HEAT EXCHANGE IN THE INNER PASSAGEWAYS OF BLADES

In engineering, the use of coarse surfaces to strengthen heat exchange is already widely in use and there are some advanced aviation engines which have blade cooling systems which also employ coarse surface inner cooling structures. The basic principle involved in coarseness strengthened heat exchange is that the coarseness interferes with the air flow and disrupts lower layer viscosity. This, as a result, lowers the resistance to heat exchange between the wall surfaces and the cooling gases. Generally, the level of

*This article was read to the 3rd Annual All-China Engineering Thermophysics Technology Conference in Qui Zhou in April of 1980.

the strengthening of the heat exchange is related to the configuration of the coarseness, the dimensions of it, the geometry of the flow path, the value of the flow body Pr and the flow Re value. What is shown in Figure 1 are the curves defined by the relationship between the heat transfer strength ratio Nu/Nu_s and the corresponding heights h/d nodal height ratios s/h. One only needs to select appropriate parameters of coarseness and it then becomes possible to effectively raise the heat transfer coefficient for the inner cavities of the blades concerned.

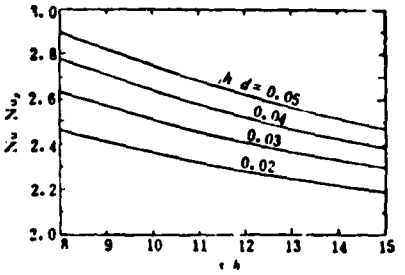

$Re = 10^5$, $Pr = 0.71$

Figure 1. Heat transfer strengthening ratios for coarsened cylinders

The cooling structures inside of blades usually take the form of unusually shaped passageways and in the acute angle sections of these passageways, it is possible to put the air flow into a laminar flow configuration. In such circumstances, the coarsened support surfaces have no strengthening effect. Because of this, it is possible to make use of horizontal supports in the vicinity of even areas, depending on flow area interference with the neighboring supports. At the same time, in the end sections of the angled areas, if one adds a concave trough in order to increase the degree of turbulence of the flow in the angled area, then one can guarantee the required strength of heat transfer.

2. THE EMPLOYMENT OF ADDITIVES TO LOWER THE TRANSFER OF HEAT FROM THE FUEL TO THE BLADES

After the combustion of a fuel that contains small amounts of $(SiOC_2H6)_n$, the SiO_2 which is produced in fuel gases whose temperatures are lower than 1700K will exist in the form of suspended particles with diameters of 0.1-1 microns. The amount of these

particles which passes through a certain integral volume surface of flow can be represented as

$$J = J_D + J_W + J_T = -D_i \operatorname{grad} n + Wn + V_T n \qquad (1)$$

In this equation J_D, J_W and J_T respectively represent the amount of molecular diffusion of particles, the amount of convection diffusion of particles and the amount of particles which are caused to move from a relatively higher temperature to a relatively lower temperature due to the effects of thermal drag in uneven temperature fields. D_i is the coefficient of diffusion of these particles in air. n is the concentration of particles. V_T is the speed of movement of the particles relative to the gas involved as induced by thermal drag.

The most important influence in the core of a turbulent flow is the amount of convection diffusion J_W. When particles follow the same air flows, they quickly diffuse. However, in viscous low layers J_W is very close to zero. To put it the other way around, J_T in the core of a turbulent flow can be ignored; however, in a viscous low layer, it becomes the deciding factor which causes the particles to precipitate out onto a cooled wall surface. According to the Epstein formula [3]

$$V_T = -(\beta\mu/\rho T) \operatorname{grad} T \qquad (2)$$

In viscous lower layers $q = -\lambda(\partial T/\partial y)_{y<\delta} = \alpha(T_w - T_g)$. From this one can obtain $(\partial T/\partial y)_{y<\delta} = \alpha(T_g - T_w)/\lambda$ and after one substitutes this into Equation (2), because of the fact that, as far as the fuel gases are concerned, $(\mu/\lambda)_{y<\delta} \approx (\mu/\lambda)_g, (\rho T)_{y<\delta} \approx \rho_g T_g$, it is finally possible to obtain the viscous lower layer precipitation speed for SiO_2 particles, which is

$$V_{TW} = -\beta(\alpha P_r/\rho C_p)_g(1 - T_w/T_g) \qquad (3)$$

The negative sign represents the direction of V_{TW} which is opposite to y. It can be seen from this that under similar conditions of temperature and pressure, the smaller the ratio value is between the wall temperature T_W and the gas flow temperature T_g, or the

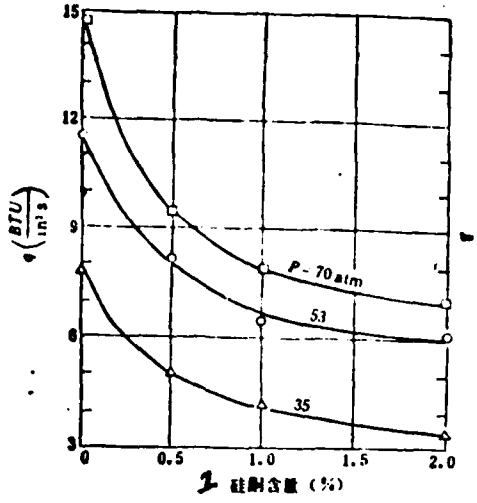

Figure 2. Heat Flow Drop in Throat Section of Jet Tube

1 - SiO_2 content (%)

larger the coefficient of heat transfer is, the greater will be the speed of precipitation of SiO_2 particles on the cool wall surfaces.

The use of additives to lower the jet tube heat flow in rocket engines has already obtained practical results. For example, the U. S. Agena lifting rocket uses a 1% addition of a silicone compound which causes on the walls of its jet tubes the formation of an active covering layer of SiO_2 and this successfully lowers the flow of heat [4]. Figure 2 displays results of the measurement of heat flow in the throat sections of jet tubes as these measurements were done in [5]. Looking from the point of view of research materials available from inside China and abroad, the addition of small amounts of additives to fuel can cause jet tube heat flow to be lowered in the neighborhood of 30-40%. The SiO_2 precipitation layer thickness in various sections of the jet tubes involved runs approximately from 0.03-0.17mm. Obviously, the larger the coefficient of heat exchange is, the larger will be the effect which is caused by the heat resistance of the SiO_2 precipitation layer on the lowering of the jet tube heat flow.

In order to do research on the effects which fuels containing carbon have on the cooling performance of high temperature turbine blades, [6] added a small amount of ethylene silicate to kerosene fuel and after combustion of this mixture, obtained temperatures of 1300-1900K. During experiments in which fuel containing SiO_2 passed through blade cascades of cooling vane blades, there was a precipitation layer of SiO_2 particles formed on the wall surfaces of the blades and this layer had a uniform thickness of 0.15mm. Because of this, experimentation and theory both demonstrate that gas flows which have small amounts of SiO_2 particles suspended in them are capable of forming a thin active covering layer on the cooling surfaces. This increases heat resistance and because of this, it is possible to reduce the transfer of heat from the fuel gas to the blades.

3. CALCULATIONS FOR THE IMPROVEMENT OF THE DESIGN OF FIRST STAGE GUIDE VANES IN MK202 ENGINES

On the basis of the design materials available concerning the first stage guide vanes of MK202 Spey engines [7], if one takes the turbine wheel intake temperature and raises it to 1600K, then the corresponding peak fuel temperature value is 1920K; the temperature and the amounts of flow of the cooling gases remain constant at 780K and 2.9%. In order to strengthen the interior cooling process in turbine blades, the flow path is changed to the structure which is shown in Figure 3. The cooling air enters from the base section of the forward cavity, then passes through the forward cavity, the middle cavity and the after cavity by way of the finned passages through them and finally, passes through a row of 0.6mm holes in the tail section of the blades concerned and it is expelled through the dish of the blades involved. On the interior wall surfaces of the blade backs and blade dishes in the cooling passageways, there are cast horizontal fins with coarse surfaces. The dimensions of these surfaces uniformly correspond to the conditions:

$h/d = 0.02$, $s/h = 10$, and the coefficient of heat exchange involved is

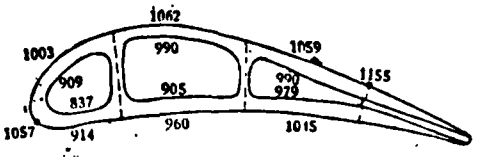

Figure 3. The internal cooling structure of guide vanes and the temperature distribution (°C) as calculated on the basis of a fuel gas temperature of 1920K

calculated on the basis of the Webb heat transfer formula coarse round tubes. Concerning the temperature rise in the cooling gases in the interior of the various passages, it is possible to assume that the interior wall temperatures along constant heights do not vary and that they are equal to the average value T_{w2i}. From these assumptions, one can deduce the calculation formula that follows, that is

$$\Delta T_{ci} = (T_{w2i} - T'_{ci})(1 - e^{-m}) \qquad (4)$$

In this equation $m = \alpha_c F_c / G_c C_{pc}$, T'_{ci} is the cooling gas intake temperature for the passage under consideration. The external heat transfer coefficient for the blades involved are selected on the basis of the sections presented in the material found in [7]. The forward station is 8710 and, as a consequence, the blade backs and blade dishes involved have their sections respectively selected as the average values shown in Figure 3. The calculations demonstrate that the highest temperatures in the tail sections of the blades start where the exhaust holes on the blade backs are located. Because of the fact that this place is the point at which the external heat transfer coefficient is at its highest in the section being considered, this coefficient is equal to 4725 kcal/m^2 hr °C. In this calculation, in the area left over, take the thickness of the SiO_2 precipitation layer to be 0.05mm and the coefficient of heat conductivity to be 0.53 kcal/m hr °C on the basis of materials

being used routinely outside of China.

Besides this, in order to improve the cooling of the forward edges of the blades concerned, make the radius of the interior arc of the forward edges equal to the external arc. This will make it easier to cause the interior and exterior heat transmission surfaces equal at the forward stations. It will also help to increase the forward edge thickness from 0.76 to 1.5mm and to cast concave troughs with coarse surfaces on the inside walls of the leading edges.

The blade temperature distribution which is calculated on the basis of these conditions is as shown in Figure 3. With the exception of the tail sections, the temperatures of all the various sections are lower than the permissible operating temperatures for the metal in the blades. If one takes the amount of the cooling gas and increases it to 4% (this is still far lower than the amount of cooling gas which is required by the standard cooling methods, that is, 6-7%) then it is possible to cause the maximum temperatures for the tail section to fall to 1081°C.

Finally, it still needs to be pointed out that the particles of SiO_2 in the fuel gases will also form precipitation on the surfaces of the moving blades. This sort of phenomenon is capable of greatly reducing the amount of cooling gas required by moving blades. The rules which govern the precipitation of these SiO_2 particles onto the surface rotor blades out to be given specialized study.

REFERENCES

[1] Gu Wei-zao; Journal of Engineering Thermophysics, 1,3, (1980)

[2] B. L. Webb et al.: Int. J. Heat Mass Trans. (1971), 601.
[3] Н. А. Фукс: Механика Аэрозолей, Изд. АН СССР, Москва, (1955).
[4] H. J. Loftus: AIAA 71—736.
[5] H. J. Loftus: et al.:AIAA 73—1289.
[6] G. N. Delyagin, Ye. M. Shvartsshteyn Heat Transfer, Sov. Res. 10, 2, (1978).
[7] RB 169-25R SPEY MK202 HP1 NGV Cooling Design Report, TBD 12001, (1976).

RESEARCH ON THE RECIRCULATING FLOW RATE IN THE WAKE OF TWO-DIMENSIONAL FLAME STABILIZERS (UNDER COLD CONDITIONS)*

Zhang Qing-fan
(Nanjing Aeronautical Institute)

THEORETICAL ANALYSIS

The recirculating flow of blunt body flame stabilizers is an important factor influencing flame stability characteristics. On the basis of jet flow theory it is possible to deduce an equation representing the recirculating flow. In Figure 1, due to the induction effects of the jets involved, the amounts of flow gradually increase. Let us assume that the properties and temperatures of the jets and ambient gases are the same. In such a case, if we do not figure in compressibility, then the total quantity of flow in jets on any plane a-a is

$$M_a = \rho_0 u_0 y_1 + \rho_0 \int_{y_1}^{y_2} u\,dy \qquad (1)$$

In this equation, ρ_0 is the jet density. u is the speed inside the jet boundary layer. On the basis of these relationships, the amount of induced jet flow within the range x is

$$M_x = M_a - \rho_0 u_0 h_0 \qquad (2)$$

In the limited jets which are shown in Figure 2, the jet boundaries and the wall surfaces intersect at F and the total quantity of jet flow on the plane x_F is

$$M_{aF} = \rho_0 u_0 y_{1F} + \rho_0 \int_{y_{aF}}^{y_{2F}} u\,dy \qquad (3)$$

In this relationship, y_{2F} is half the height of the passage involved.

*This paper was read at the 3rd Annual All-China Engineering Thermophysics Technology Conference in Gui Zhou in April of 1980.

On the basis of this, the largest amount of induced jet flow in the two-dimensional passage involved is

$$M_{cmax} = M_{xF} = \rho_0 u_0 h_0 \qquad (4)$$

The gases of the jet flow which is induced by the limited jets involved here form in the tube exhaust a secondary flow, the speed of which is u_s. Experiments demonstrate that when the amount of flow involved in this secondary flow is smaller than the amount of induced flow in Equation (4), one will see the initial formation of a reflux flow first in the vicinity of point F. The smaller the amount of flow involved in the secondary flow is, the larger the area of the reflux flow will be. When the secondary flow is equal to zero, the amount of induced jet flow is equal to the amount of reflux flow. In such a circumstance, the dimensions of the area of reflux flow are at their largest, filling the entire exterior part of the passage. This is equivalent to the exterior part of the passage being blocked (Figure 3). If one does not figure in the friction between the gas flow and the wall surfaces involved, then the boundary conditions for Figure 3 and Figure 4 are the same. Because of this, one can replace Figure 3 and take the height of the passage B as half the trough width of the stabilizer. It can be seen that the amount of flow from the stabilizer is related to the calculated values of Equation (4).

If the flow characteristics of limited jets and free jets are the same, then it is possible to directly employ the boundary lines presented in the first section of the related equations in [2], that is

$$y_1 = h_0 - 0.416b \qquad (5)$$

The external boundary line for the initial stage

$$y_2 = h_0 + 0.584b \qquad (6)$$

The jet boundary layer width

$$b = y_2 - y_1 = cx \qquad (7)$$

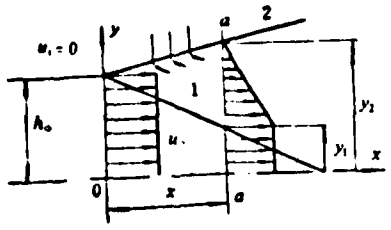

Figure 1. A simplified diagram of a free planer jet flow

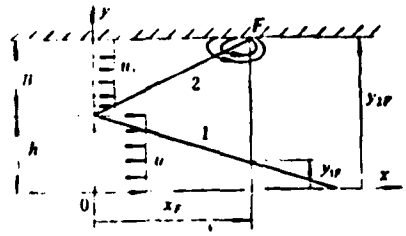

Figure 2. A simplified diagram of limited planar jet flow

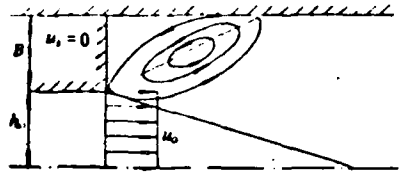

Figure 3. Planar Limited Jet When $u_s = 0$

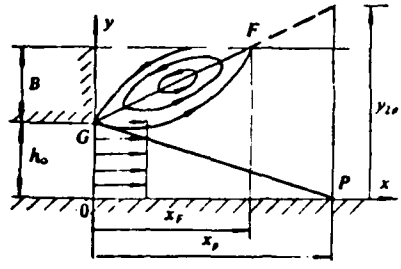

Figure 4. Two Dimensional Flame Stabilizer Wake Flow

In this equation, c is a coefficient. The speed distribution for the interior of the boundary layers involved is

$$(u_0 - u)/u_0 = (1 - \eta^{1.5})^2 \qquad (8)$$

In this equation, η is a non-dimensional coordinate and is also defined by the equation

$$\eta = (y_2 - y)/b \qquad (9)$$

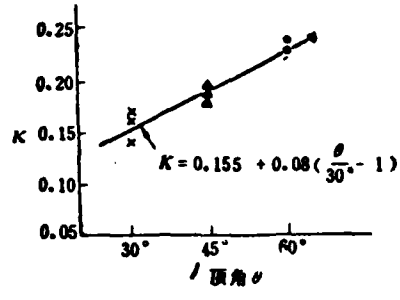

Figure 5. The relationship between the coefficient K and the geometrical parameters of stabilizer devices.
Key: 1--apex angle

One can take the Equations (5)-(9) and substitute them into Equation (3). Then one can solve for the maximum amount of induced jet flow from Equation (4), that is

$$M_e/\rho_0 h_0 u_0 = 0.23 B/h_0 \tag{10}$$

Equation (10) represents the induced flow energy from a limited jet when the secondary flow is sufficiently large (no reflux flow). However, when the secondary flow is zero, the flow conditions at the boundaries of the jet flow begin to change, and this is particularly true of the blockage ratio of the stabilizer apparatus, that is $\varepsilon = B/(B + h_0)$. Therefore, the actual amount of reflux flow is M_r, or

$$M_r/\rho_0 h_0 u_0 = K\varepsilon/(1 - \varepsilon) \tag{11}$$

This is nothing else but the equation representing the amount of reflux flow as that amount can be deduced from the theory of jets. The coefficient K in this equation can be fixed to a precise value by experimentation.

METHODS AND RESULTS OF EXPERIMENTATION

Concerning the measurement of the parameters of the reflux flow area in a cold condition, the dimensions of the transparent two-dimensional passage are 100x150mm^2. The length of the stabilizer device is 100mm. The average flow speed in front of the stabilizer device is 34m/s. By the use of normal total pressure values and round dish investigation techniques we can respectively determine the reflux flow area total static pressure and the reflux flow introduced in the lower sections to be the largest amounts of reflux flow in the center cross sections. The experimental results for three types of blockage ratios and three types of apex angles for each of nine types of stabilizer devices are presented in Figure 5. From this one can obtain the K value for Equation (11), which is

$$K = 0.155 + 0.08(\theta/30° - 1) \tag{12}$$

In this equation θ is the apex angle of the stabilizer device (degrees). On the basis of this, according to the theory of jets,

one can deduce the amount of reflux flow from a two-dimensional stabilizer device in a cold condition, that is

$$M_r/M_a = [0.155 + 0.08(\theta/30° - 1)]\varepsilon/(1-\varepsilon) \quad (13)$$

In this equation, M_a is the total quantity of flow over the stabilizer device. The appropriate range for use with Equation (13) is this: stabilizer device blockage ratio 0.2-0.4, and stabilizer device apex angle 30-60°. The Reynolds number defined by the width of the trough is $(0.7\text{-}1.4)\times10^5$. This article does not contain any research into the influence of the degree of turbulence in a flow and because of this, strictly speaking, the results obtained are only suitable for use under experimental conditions in which there are specially determined Reynolds numbers.

REFERENCES

[1] Curtet, R: Confined jets and recirculation phenomena With cold air, *Combustion and flame*, 2, (1958).

[2] Xie Xiang-chun; "The Theory and Calculation of Turbulent Flows", Science Publishing House, 1975

A NEW METHOD OF COOLING TURBINE VANES

Gu Wei-zao, Zhang Yu-ming, Xu Hong-kun

(Institute of Engineering Thermophysics, Academia Sinica)

Abstract

In this paper the methods of augmentation of convective heat transfer in the cooling channels of the vane with rough surface and formation of the dynamic coating on the airfoil surface in virtue of silicone additives in the fuel were suggested. By means of these could be raised the turbine inlet gas temperature to 1600 K when coolant to gas flow ratio is equal to 0.03–0.04.